MICROCOPY RESOLUTION TEST CHART

NATIONAL BUREAU OF STANDARDS-1963-A

$E301841$

AD-A162 164
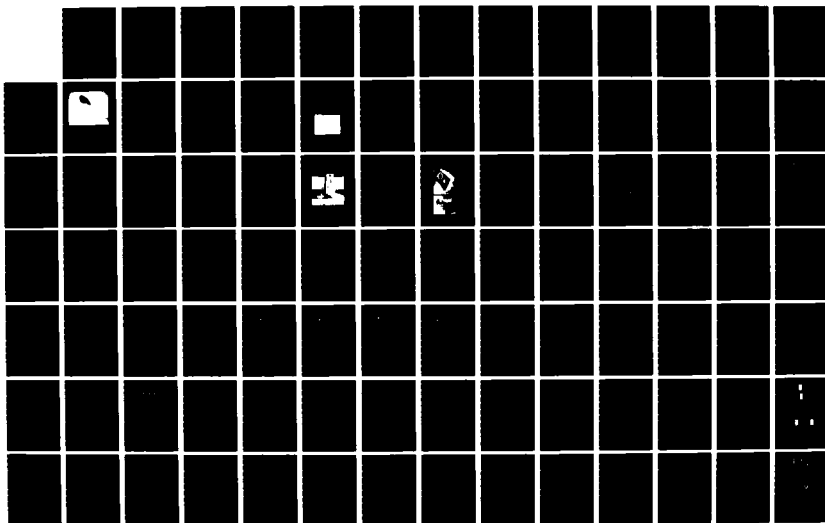
DNA-TR-84-332

THE DESIGN, FABRICATION AND FIELD TESTING OF A GAS PARTICLE VELOCITY SENSOR

Eldine Cole
Glenn Roark
Kaman Sciences Corporation
P.O. Box 7463
Colorado Springs, CO 80933-7463

31 August 1984

Technical Report

DTIC
ELECTE
NOV 2 9 1985

A

Prepared for
Director
DEFENSE NUCLEAR AGENCY
Washington, DC 20305-1000

85 9 09 014

AD-A162164

REPORT DOCUMENTATION PAGE

1a. REPORT SECURITY CLASSIFICATION UNCLASSIFIED	1b. RESTRICTIVE MARKINGS
2a. SECURITY CLASSIFICATION AUTHORITY	3. DISTRIBUTION/AVAILABILITY OF REPORT
2b. DECLASSIFICATION/DOWNGRADING SCHEDULE N/A since UNCLASSIFIED	Approved for public release; distribution is unlimited.
4. PERFORMING ORGANIZATION REPORT NUMBER(S) K84-126U(R)	5. MONITORING ORGANIZATION REPORT NUMBER(S) DNA-TR-84-332

6a. NAME OF PERFORMING ORGANIZATION Kaman Sciences Corporation	6b. OFFICE SYMBOL (If applicable)	7a. NAME OF MONITORING ORGANIZATION Director Defense Nuclear Agency
6c. ADDRESS (City, State, and ZIP Code) P.O. Box 7463 Colorado Springs, CO 80933-7463		7b. ADDRESS (City, State, and ZIP Code) Washington, DC 20305-1000
8a. NAME OF FUNDING/SPONSORING ORGANIZATION	8b. OFFICE SYMBOL (If applicable)	9. PROCUREMENT INSTRUMENT IDENTIFICATION NUMBER DNA 001-82-C-0140

8c. ADDRESS (City, State, and ZIP Code)	10. SOURCE OF FUNDING NUMBERS			
	PROGRAM ELEMENT NO. 62715H	PROJECT NO. H11CAXS	TASK NO. X	WORK UNIT ACCESSION NO. DH005972

11. TITLE (Include Security Classification)
THE DESIGN, FABRICATION AND FIELD TESTING OF A GAS PARTICLE VELOCITY SENSOR

12. PERSONAL AUTHOR(S)
Eldine Cole and Glenn Roark

13a. TYPE OF REPORT Technical	13b. TIME COVERED FROM 820416 TO 840523	14. DATE OF REPORT (Year, Month, Day) 840831	15. PAGE COUNT 96

16. SUPPLEMENTARY NOTATION
This work was sponsored by the Defense Nuclear Agency under RDT&E RMSS Code
B344082466 H11CAXSX00006 H2590D.

17.	COSATI CODES		18. SUBJECT TERMS (Continue on reverse if necessary and identify by block number)
FIELD	GROUP	SUB-GROUP	Vortex Shedding Anemometer Shock Tube Flow
18	3		Gas Particle Velocimeter
15	2		Air Blast Velocimetry

19. ABSTRACT (Continue on reverse if necessary and identify by block number)

The vortex shedding anemometer (VSA) was developed by Kaman Sciences Corporation (ca. 1967) for measuring transient gas particle velocity in the flow behind an air shock wave. The original VSA was calibrated up to Mach 1 where the minimum response time was on the order of 700 microseconds.

A higher velocity model has been designed and tested up to Mach 2.2 with a response time approaching 100 microseconds. This new device was calibrated in the quasi-steady state flow field of a transonic wind tunnel and in the transient flow in a shock tube. Four devices were fielded on test event DIRECT COURSE at the 240 kPa (35 psi) predicted overpressure level. Unfortunately, no unambiguous velocity measurements were recorded on this test due to interchannel modulation cross talk in the multiplexed recording system.

20. DISTRIBUTION/AVAILABILITY OF ABSTRACT ☐ UNCLASSIFIED/UNLIMITED ☒ SAME AS RPT. ☐ DTIC USERS	21. ABSTRACT SECURITY CLASSIFICATION UNCLASSIFIED	
22a. NAME OF RESPONSIBLE INDIVIDUAL Betty L. Fox	22b. TELEPHONE (Include Area Code) 202 325-7042	22c. OFFICE SYMBOL DNA/STTI

DD FORM 1473, 84 MAR   83 APR edition may be used until exhausted.
All other editions are obsolete.

PREFACE

CONVERSION TABLE
(Symbols of SI units given in parentheses)

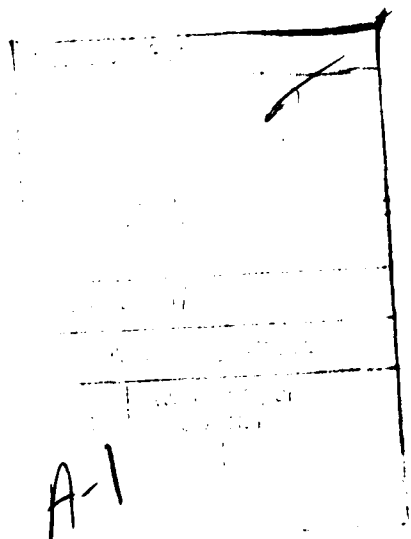| To Convert From	To	Multiply By
angstrom	meter (m)	1.000 000*E-10
atmosphere (normal)	pascal (Pa)	1.013 25 E+05
bar	pascal (Pa)	1.000 000*E+05
British thermal unit (thermochemical)	joule (J)	1.054 350 E+03
Btu (thermochemical)/foot^2-second	watt/metre^2 (W/m^2)	1.134 893 E+04
cal (thermochemical)/cm^2·s	watt/metre^2 (W/m^2)	4.184 000*E+04
centimeter of mecury (0 C)	pascal (Pa)	1.333 22 E+03
centimeter of water (4 C)	pascal (Pa)	9.806 38 E+01
decibar	pascal (Pa)	1.000 000*E+04
degree Celsius	kelvin (K)	$t_k = t_c + 273.15$
degree Fahrenheit	degree Celsius	$t_c = (t_f - 32)/1.8$
dyne	newton (N)	1.000 000*E-05
dyne-centimetre	newton-metre (N·m)	1.000 000*E-07
dyne/centimetre^2	pascal (Pa)	1.000 000*E-01
erg	joule (J)	1.000 000*E-07
foot	metre (m)	3.048 000*E-01
foot of water (39.2 F)	pascal (Pa)	2.988 98 E+03
gram/centimetre^3	kilogram/metre^3 (kg/m^3)	1.000 000*E+03
gram-force/centimetre^2	pascal (Pa)	9.806 650*E+01
inch	metre (m)	2.540 000*E-02
inch of mecury (32 F)	pascal (Pa)	3.386 389 E+03
inch of water (39.2 F)	pascal (Pa)	2.490 82 E+02
kilocalorie (International Table)	joule (J)	4.186 800*E+03
kilocalorie (thermochemical)/second	watt (W)	4.184 000*E+03
kilogram-force (kgf)	newton (N)	9.806 650*E+00
kilogram-force-second^2/metre (mass)	kilogram (kg)	9.806 650*E+00
kip (1000 lbf)	newton (N)	4.448 222 E+03
kip/inch^2 (ksi)	pascal (Pa)	6.894 757 E+06
mile (U.S. statute)	metre (m)	1.609 344*E+03
millibar	pascal (Pa)	1.000 000*E+02
millimetre of mecury (0 C)	pascal (Pa)	1.333 224 E+02
pound-force/inch^2 (psi)	pascal (Pa)	6.894 757 E+03
ton (nuclear equivalent of TNT)	joule (J)	4.20 E+09

QUALITY INSPECTED 3

2

A-1

TABLE OF CONTENTS

LIST OF ILLUSTRATIONS

LIST OF ILLUSTRATIONS (Continued)

6

SECTION 1
INTRODUCTION

1.1 MEASUREMENT REQUIREMENT

Proper interpretation of observed effects from an airblast requires adequate definition of the significant environmental parameters. The Defense Nuclear Agency (DNA) is especially concerned with accurate measurement of these parameters during field tests designed to simulate the airblast environment from a nuclear explosion.

Dynamic pressure is important in studies relating to drag loading and forces on a target that is subjected to airblast. Measurement of dynamic pressure remains as a difficult challenge.

The component of stagnation pressure that arises from the kinetic energy of the mass flow is known as dynamic pressure. It is commonly denoted by the symbol "q" and is defined by the relationship:

$$q = \frac{1}{2} \rho u^2 \qquad (1)$$

where ρ is the gas density and u is the gas particle velocity in free stream flow. The dynamic pressure is not measured directly but is a computed value derived from measurements of other parameters.

The Rankine-Hugoniot relationships[1] for ideal gases are used with measurements of static overpressure, total or stagnation pressure and shock wave Mach number to calculate dynamic pressure. Extension of this theory to nonidealized flow conditions gives rise to very large uncertainties in the answers so derived.

7

One obvious approach for determination of q would be to measure ρ, the density and u, the velocity directly and then compute dynamic pressure from its defining equation. While this may be a fine concept, very limited means exist for measurement of these two quantities in a field application. The beta-ray densitometer[2,3] measures gas density but it is also sensitive to the level of entrained dust concentration. A method of measuring density that is sensitive to only dust or gas is needed to compliment the beta-ray densitometer measurement and allow for separation of these two quantities.

1.2 HISTORICAL BACKGROUND

The Vortex-Shedding Anemometer (VSA)[4] was developed to fill the need for a blast-hardened sensor for measurement of the gas particle velocity.

Working under the auspices of the Defense Atomic Support Agency (DASA) under contract DA49-146-XZ-328, FS49-146-SZ-548, and DASA01-67-C-0111 (Ca. 1965-1967), Kaman Sciences Corporation (KSC) (then Kaman Nuclear) first developed a rapid response anemometer and later incorporated two of these devices into a portable, four-channel blast instrumentation system. The instrumentation system provided dual channels for measurement of pressure and velocity profiles in the subsonic flow regime up to Mach 1. This allowed operation of the system up to peak blast overpressure levels of approximately 35 psig.

After completion of these blast instrumentation systems, construction work was completed on the explosives-driven large conical shock tube, DASACON, at the Naval Weapons Laboratory in Dahlgren, Virginia (now NSWC-Dahlgren). This facility used the KSC designed and fabricated anemometer systems for the measurement of the air particle speed profiles during the shakedown and calibration phase of implementing this facility.

8

The VSA was subsequently used to measure particle speed at a range of 149 meters from a 20-ton TNT charge in Operation DISTANT PLAIN[5]. Figure 1 shows the reduced data obtained from that test.
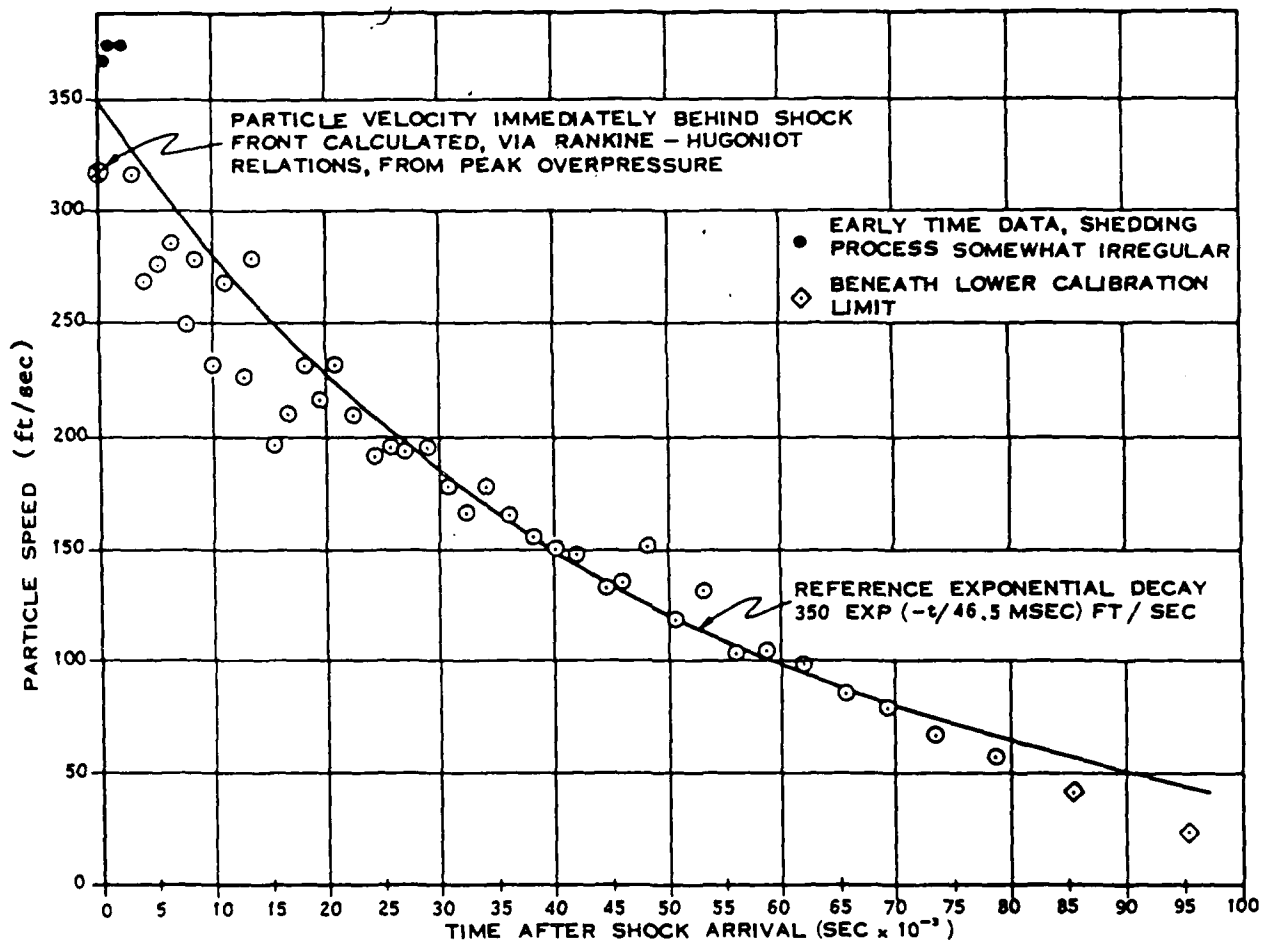
Figure 1. Derived from VSA transducer output (20-ton TNT charge - radius to ground zero 149m) Operation DISTANT PLAIN.

9

The pressure step at the shock front can be used to calculate the particle velocity immediately behind the shock front. This data should substantiate the VSA data in the region of the shock front. This calculation has been done assuming ideal gas properties for air at standard sea level conditions. The results appear in Figure 2.
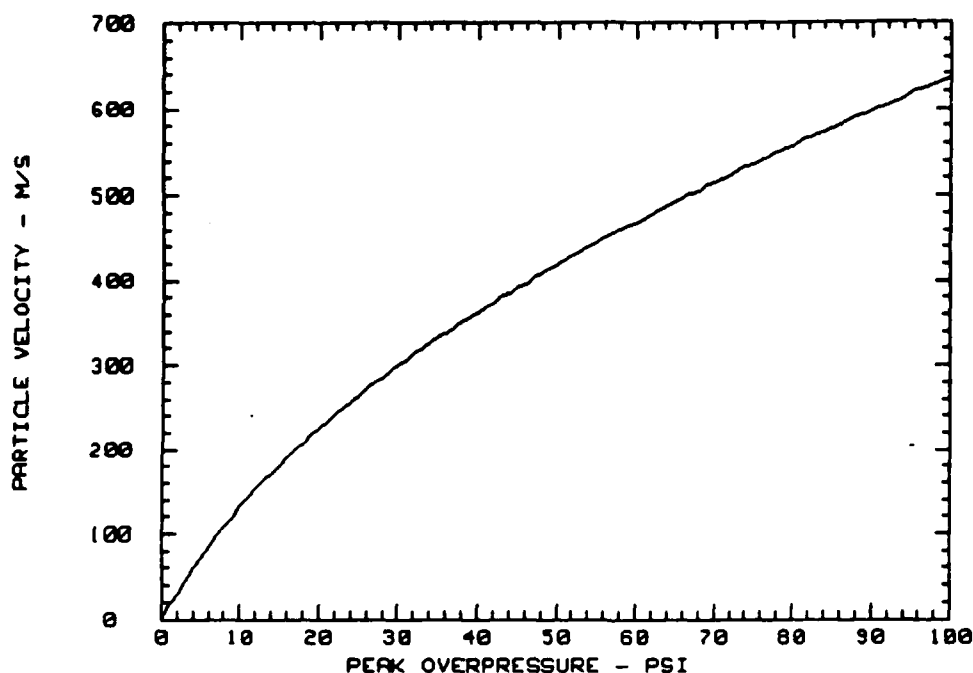
Figure 2. Relationship between air shock overpressure and particle velocity at sea level (assuming ideal gas relationships).

A photograph of the original model VSA is shown in Figure 3. The top cover has been removed to expose the vortex generating right circular cylinder and the two probes for pressure measurement.

Figure 3. Anemometer with top cover removed showing
flow obstruction and transducer probes.

The original VSA was calibrated under steady state flow conditions in the subsonic and transonic wind tunnels at the United States Air Force Academy (USAFA), Colorado.

11

SECTION 2
DESIGN OBJECTIVES

Contractual tasks as taken from the DNA 001-82-C-140 Scope of Work are as follows:

Task 1. Design, fabricate, and calibrate advanced development models of the Vortex Shedding Anemometer.

Task 2. The frequency response of the existing VSA will be improved by at least a factor of 4.

Task 3. Evaluate the feasibility of extending the useable velocity range from less than Mach 1 to Mach 1.5.

Task 4. Investigate the sensitivity of the VSA to environmental factors. Also investigate the options and trade offs related to preprocessing raw data signals and recording options.

Task 5. Package the VSA signal conditioning electronics for use in the normally expected environment of a field test.

Task 6. Deliver two each advanced development type models of Vortex Shedding Anemometer.

Task 7. Fabricate two additional airblast sensors of the same design as developed in the basic contract.

Task 8. Design and fabricate four field mounts for the four airblast sensors.

Task 9. Interface with DNAFC and DNA Airblast Recording Group as required.

Task 10. Reduce the test data provided by DNA to engineering units.

All of these tasks have been accomplished and are reported in the remainder of this document.

SECTION 3
VSA DESCRIPTION

3.1 THEORY OF OPERATION

An obstruction placed in a viscous fluid flow causes a vortex pattern to be formed in its wake. Vortices are formed from both sides of the obstruction. This phenomenon is illustrated for an obstruction with circular symmetry in Figure 4. A visualization of the vortex shedding process is possible with the aid of a smoke tunnel that injects smoke trails into the flow stream lines. Figure 5 is a photograph showing the formation of vortices in the wake of a cylinder in this flow. Note the phase similarity as both figures portray the same moment in time.

The side-by-side vortex configuration shown is unstable and the vortices periodically separate from the obstruction and are swept down-stream in the wake. The separation occurs alternately from one side and the other. It takes place at a frequency, f_s, which is a function of the free stream velocity, u, a characteristic dimension, d, and a dimensionless quantity, S, known as the Strouhal number, such that $f_s = Su/d$. The Strouhal number is nearly a constant for a given obstruction shape over a wide range of Reynolds numbers. A right circular cylinder is used in the VSA as the obstruction to generate vortices.

Pressure inlet ports are positioned downstream from the cylinder so that one port is centered in the vortex while the other is peripherally located. This results in a differential measurement with maximum out-of-phase pressure fluctuations.

The frequency of the vortex shedding phenomena is seen to be a function of the free stream velocity. Typically, a steady vortex separation process is established within a few cycles. An upper

14
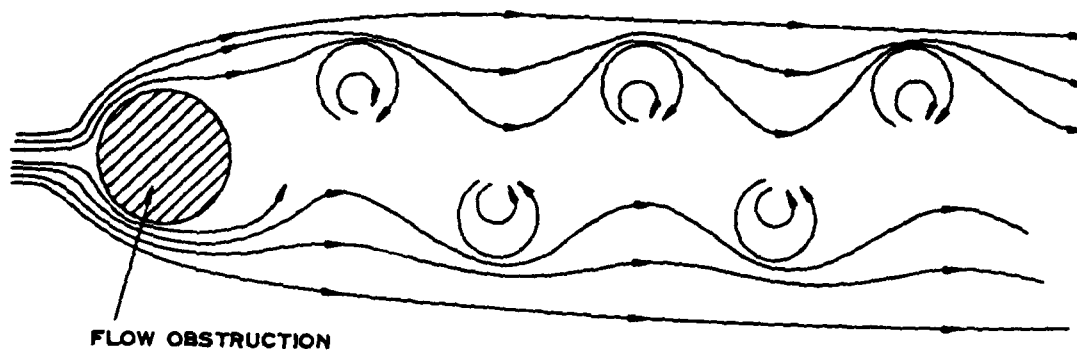
FLOW OBSTRUCTION

Figure 4.   Flow diagram of a stable vortex street.
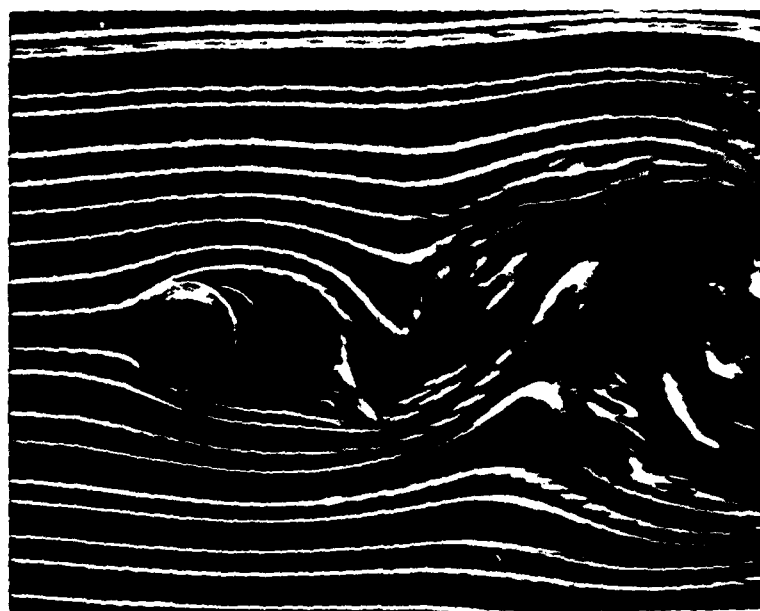
Figure 5.   Smoke trail photograph of fluctuating wake.

15

bound on the frequency response may be established quickly, since in no case is it possible to measure the frequency in less than one cycle. The exact response time to establish steady vortex shedding depends upon the turbulence of the gas and the shedding frequency (i.e., velocity).

Two notable limitations of the original VSA design were found in the response time and the upper useful Mach number range. Both of these items were addressed for improvement in the new design.

The shedding frequency is inversely proportional to the diameter of the obstruction. Since a rapid response requires a high shedding frequency, response time considerations dictate a small obstruction size.

The diameter of the vortex generator used in the original model is 16.9 millimeters which defines the shedding frequency (f_s) at any given velocity. With reference to theory presented, the frequency will be increased for a given velocity if the diameter is reduced. While the particle velocity information is recognized to be contained in the frequency, the pressure amplitude of the vortex signal is also velocity dependent. As the cylinder diameter is decreased, the magnitude of the pressure fluctuations in the vortices is also decreased. This results in a loss of sensitivity at lower velocities or a requirement for a more sensitive pressure transducer.

As the diameter is decreased, the sensitivity of the pressure transducer must be increased, however the relationship is not linear. Early experimental results during development of the VSA showed a 25% reduction in pressure for a 4:1 diameter decrease. Thus, by taking advantage of miniaturization in pressure sensor size, a new design was proposed that could provide the desired faster response time and was potentially capable of operation at Mach numbers in excess of one.

3.2 VSA DESIGN

Design details for the original model VSA are included in this report along with those for the advanced development model. Dimensions for both the original and advanced development model are given in Figure 6. The newer model does not replace the original model but rather compliments it by adding an instrument with different specifications. The experience and insight gained during development and testing of the most recent version has provided enough information to confidently design a VSA taylored to specifications for applications ranging from Mach 1.6 or more down to velocities of less than one meter per second.
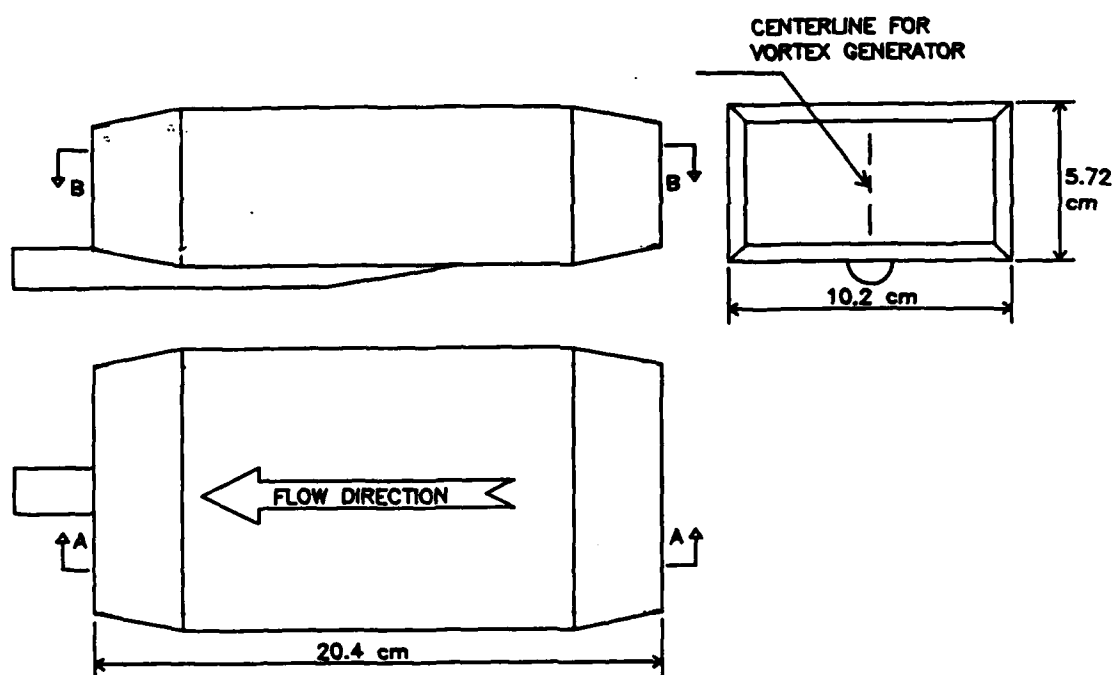
Figure 6. Outline drawing of VSA probe housing.

The VSA probe housing serves two important functions. First it provides for a rigid, nonresonant support to the vortex generating obstruction with protective channels for routing the transducer wiring out of the blast environment. This support is especially important for the small slender rod used in the newer model.

The housing box also provides a two-dimensional flow field around the vortex pressure generator, thus avoiding the distortion that would result from flow over the top of a free standing obstruction.

There is evidence that the probe housing may also have choked the flow velocity during the steady state wind tunnel calibrations above Mach 1. Refer to Section 3.3 for more on this topic.

3.2.1 Frequency Response

The two models will be referenced in this report as the low velocity VSA (LV-VSA) and the high velocity VSA (HV-VSA). Each design model has its own special features that make it preferable for given applications.

The LV-VSA is recommended for velocity measurements on large charge high explosives (HE) tests that typically generate a positive pressure lasting for many tens of milliseconds. The HV-VSA design is more appropriate for tracking the flow velocity from the smaller HE charges where the measurement stations are necessarily closer to the source to obtain any given peak overpressure and the positive phase duration lasts for only a few milliseconds.

Generally, the LV-VSA is more rugged and will survive a more hostile environment but at the sacrifice of frequency response. Fortunately, the large yield tests do not require the high frequency response required for the small shots. Orientation of the

18

pressure sensing ports on the LV-VSA is also preferable for dusty flow because they do not face directly into the flow. This provides less opportunity for damage to the pressure sensor or clogging of the ports.

Figure 7 shows two views of the LV-VSA internal design. The differential pressure transducer which also functions as the vortex generator is a special KSC model with acoustically tuned inlet ports for flat amplitude response over the calibrated frequency range of the instrument.

SIDE VIEW (SECTION A—A)

TOP VIEW (SECTION B—B)
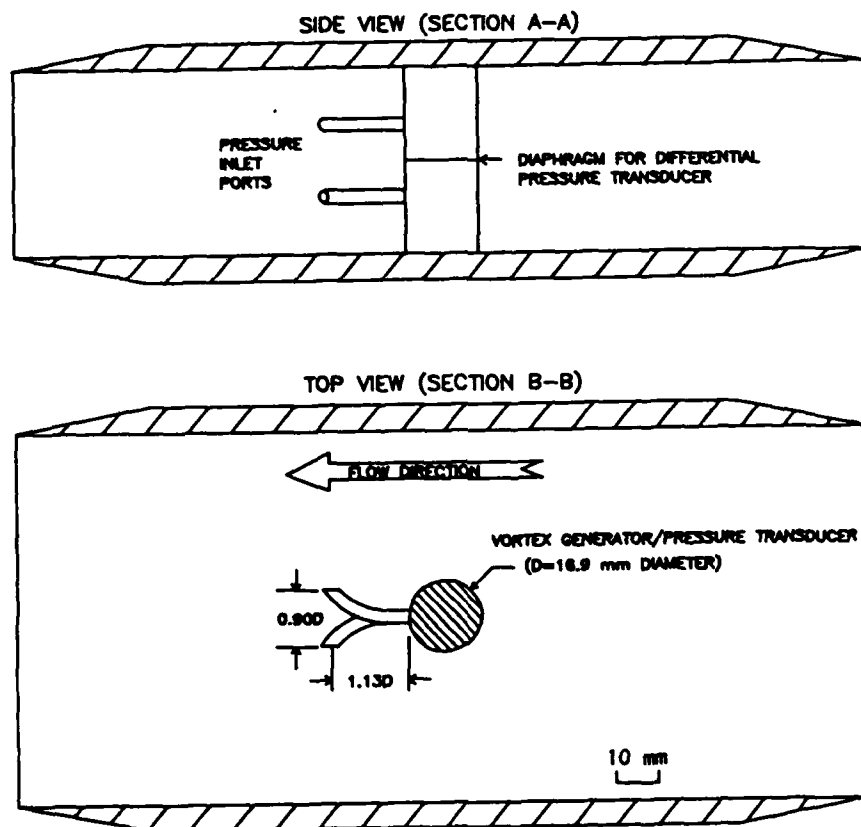
Figure 7. Views of LV-VSA.

The HV-VSA with its intrinsically higher frequency response
is also more vulnerable to damage from dust and debris. The
higher frequency response is obtained by reducing the diameter of
the vortex generating obstruction. The smaller diameter precludes
installation of the pressure transducer in the obstruction because
of physical size constraints. The downstream placement of the
ports on an external mounting wedge is shown in Figure 8. Note
that they face upstream. Thus, not only are the components more
delicate due to reduced size but the position of the pressure
sensing ports is more susceptable to debris damage and dust
collection.

SIDE VIEW (SECTION A-A)

TOP VIEW (SECTION B-B)

FLOW DIRECTION

1.30D

VORTEX GENERATOR
(D=4.2 mm DIAMETER)

PRESSURE TRANSDUCERS (2 ea)
KULITE XCQ-062-100SG
1.6 mm DIAMETER

2.5D

10 mm

Figure 8. Views of HV-VSA.

Frequency response of the VSA is directly coupled to the flow velocity due to the proportional relationship between shedding frequency and velocity. The LV-VSA calibration was seen to have a shedding frequency of 2700 Hz at 310 m/s flow velocity which implies one frequency sample each 370 microseconds. The calibration curve for the HV-VSA will show this model to have a shedding frequency of 10 kHz for the same free stream velocity. This number translates to one frequency sample each 100 microseconds. The HV-VSA was calibrated at a maximum velocity of 515 m/s with a corresponding frequency of 14.25 kHz giving a 70 microsecond sampling interval.

These values establish an upper limit on the transient response time for these VSA models. Actual response times will be dependent on the level of turbulence and the clearing times required to establish quasi-steady flow behind the vortex generating obstruction.
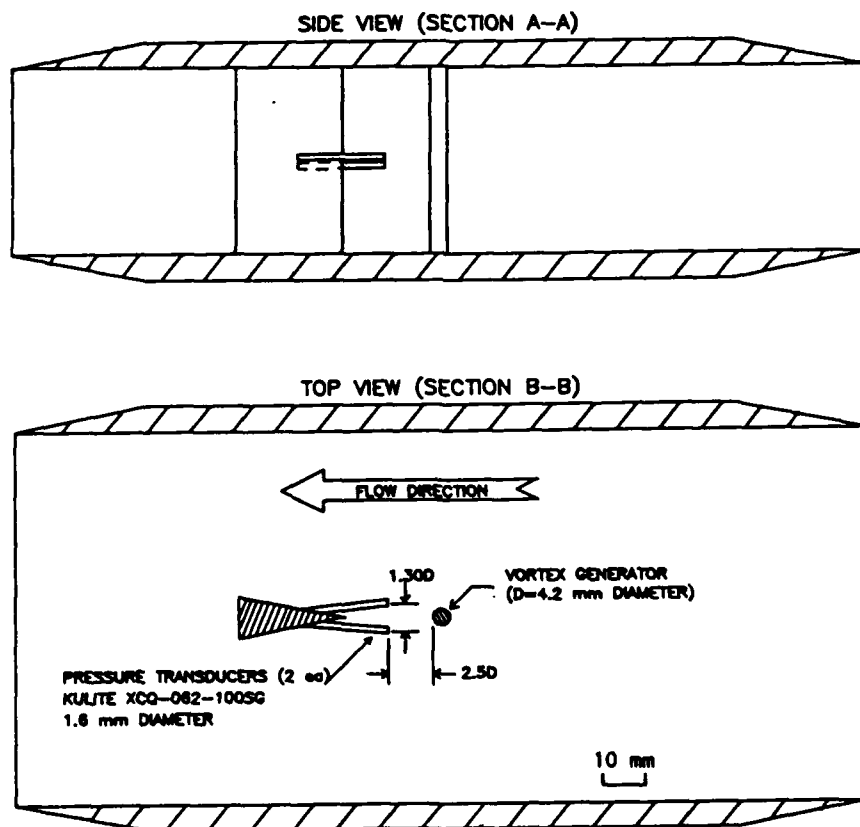
3.2.2 Velocity Range

In tests performed with the original instrument, there were encouraging indications of velocity dependent wake fluctuations at speeds in excess of Mach 1.0. These were masked by the presence of a velocity independent signal which was more than 10 dB stronger than the one being observed. Spectral analysis was required to establish the presence of the signal being used to indicate velocity. By use of a device such as a tracking filter, there was promise that continuously varying velocity dependent signals could be selected in the presence of high background interference. Techniques for data processing of this nature would likely be most effectively utilized during playback of recorded data from magnetic tapes.

21

Figure 9 shows spectral density plots of the original transducer output signal showing the progressive development of an interference signal as the Mach number is increased. Note the absence of any interference signal for M = 0.90 in Figure 9, the the appearance of a weak signal for M = 0.98 and finally, the predominance of interference at M = 1.15. Although the signal of interest is swamped out with the alien frequency it is possible with spectral analysis to observe the 3350 Hz component that is velocity dependent.
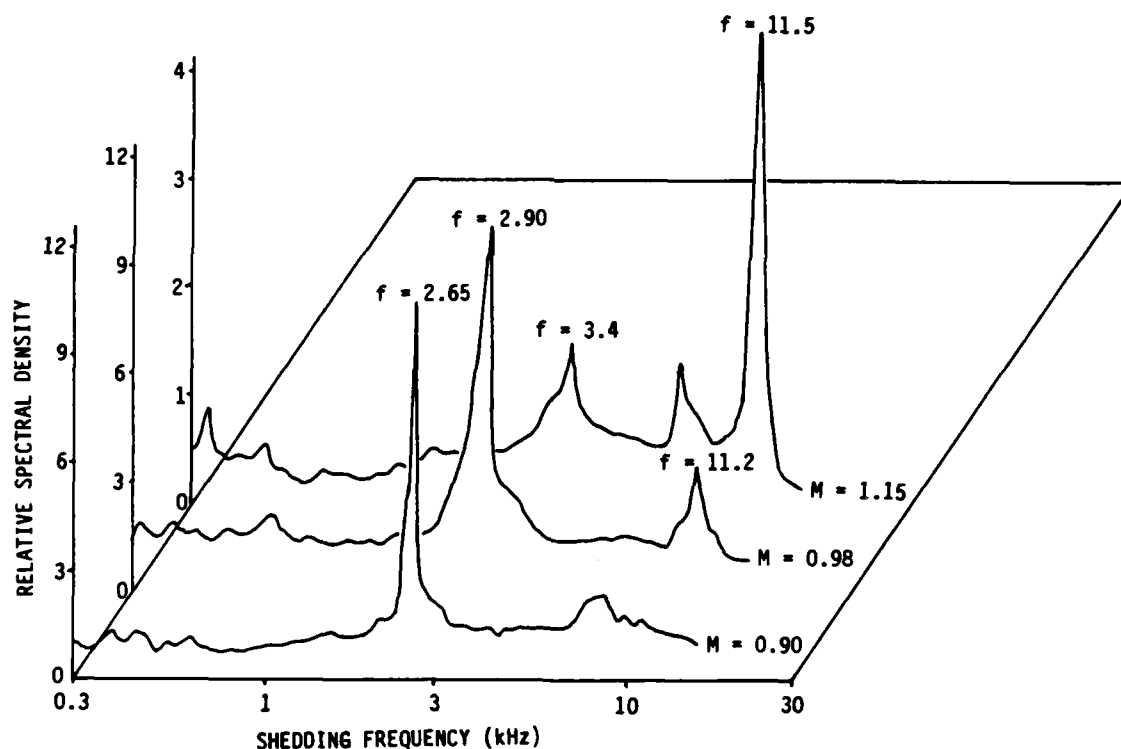

Figure 9. Spectral composition of VSA signals.

Upon further investigation, we believe that the interference signal may have been caused by the VSA sensor detecting secondary vortex shedding from the 1/8-inch tubing used as sensing ports. The changing velocity caused a shift in flow pattern around the vortex generator which likely placed the end of the tubes too far away from the optimum location to detect the primary vortex shedding and the secondary shedding frequency from the sensing ports dominated the signal. This problem was circumvented on the High-Velocity VSA by installation of the detecting probes on a wedge located downstream from the vortex generator. There is reason to believe that the LV-VSA would also function above Mach 1 if the pressure ports were positioned differently.

3.2.3 Gas Density Effects

No effects of gas density changes have been observed on the calibration when testing with clean air over a density range from 0.16 to 2.6 gram/liter. Experimental results reported[6] show the Strouhal number to remain relatively constant at 0.2 (+1, -4%) over a range of Reynolds numbers from 500 to 100,000. The relationship between these two parameters was unchanged when tested over a wide range of density ratios from 70 to 1, again in clean air flow.

3.2.4 Dusty Shock Waves

Since the VSA may be used where dust is entrained in the flow behind the shock front, the effect of dust on the measurement is of interest. It is assumed that the principal effect of dust is to change the Reynolds number for a specific flow rate. The Reynolds number R relates to the gas parameters and a bluff body

$$R = ud \left(\frac{\rho}{\eta}\right) \tag{2}$$

where ρ = gas density, u = flow velocity, d = diameter of the bluff body, and η = the gas viscosity. The vortex frequency of

23

the VSA is somewhat independent of Reynolds number over a wide range of velocities of interest.

Note that the dust effects the $\left(\frac{\rho}{\eta}\right)$ term. To significantly affect the gage performance at the velocities of principle interest would require the $\left(\frac{\rho}{\eta}\right)$ term to decrease by a factor of greater than 25. This would require a very significant increase in viscosity since gas density is relatively insensitive to moderate dust levels.

The VSA has been observed to be very insensitive to changes in gas density which implies that the vortex shedding mechanism is not closely coupled to sonic velocity changes that might result from dust entrained in the air. Flow velocity changes caused by energy interchange between dust and air would obviously be expected to be indicated by the VSA as the instrument sensed a change in rate of vortex shedding consequent to a flow velocity change.

Thus, a preliminary review of the basic operating principles of the VSA indicate probable immunity from dust effects for shock wave particle velocities greater than 100 m/sec ($\Delta P > 6$ psi) and moderate dust levels. A more quantitative evaluation of dust effects on VSA performance remains to be investigated.

3.3 CALIBRATION

The original VSA concept was developed in the USAFA subsonic wind tunnel which is a closed loop with a maximum flow velocity of 100 m/s. Calibration up to Mach 0.98 was performed in their transonic tunnel. The results of this calibration for the LV-VSA are given in Figure 10 showing approximate linearity up to 150 m/s and excellent correlation to a third order polynomial over the entire range. Observe that the data between the two wind tunnels overlap, although the subsonic tunnel operates at one atmosphere and the transonic tunnel operates at two atmospheres pressure.

24
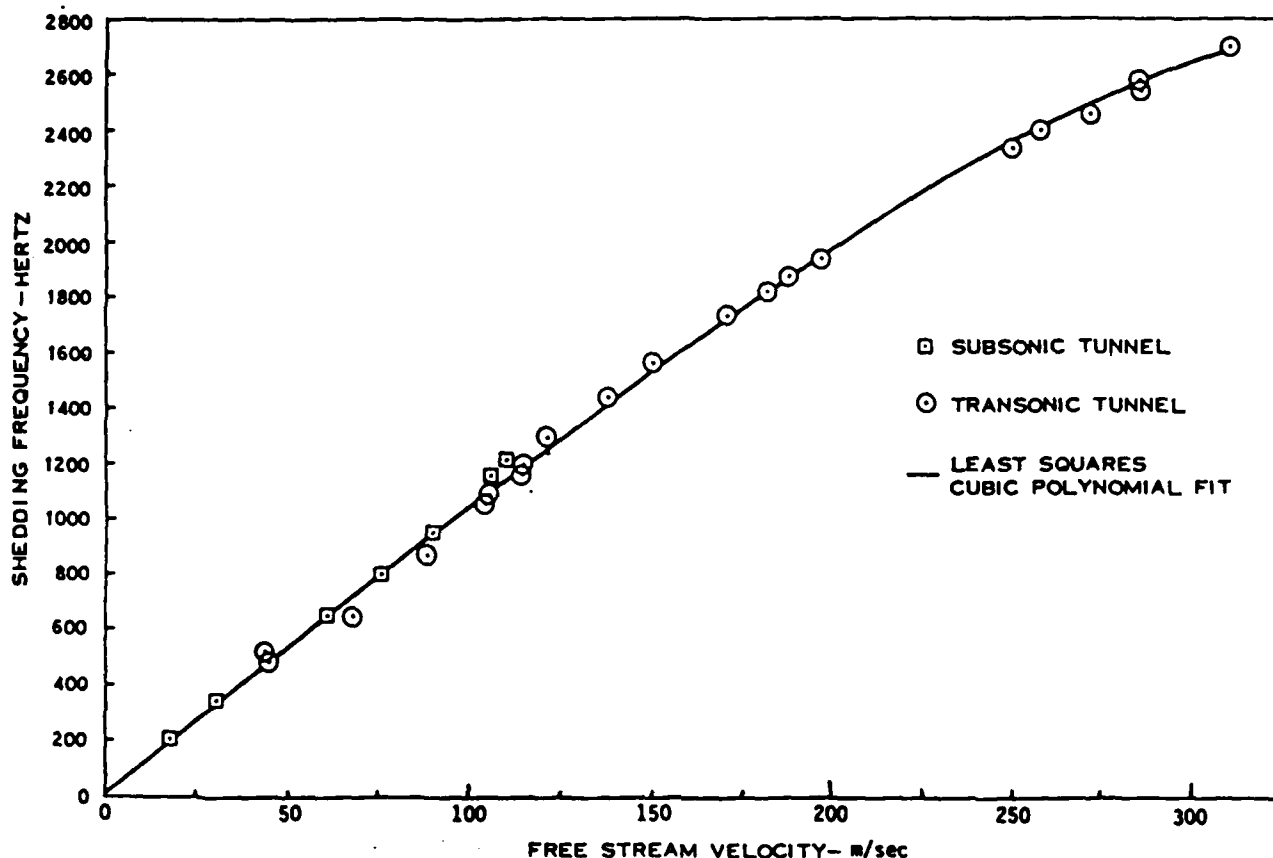
Figure 10. Calibration of the LV-VSA.

The currently developed HV-VSA was calibrated in the quasi-steady state flow conditions of the USAFA transonic wind tunnel up to Mach 1.67. Additionally, it was tested and calibrated under transient flow conditions in the 24 inch shock tube at Ballistics Research Laboratories, Aberdeen, MD. Data from these calibrations have all been plotted in Figure 11. The LV-VSA data from Figure 10 also have been overlayed for comparison of the two models.

25
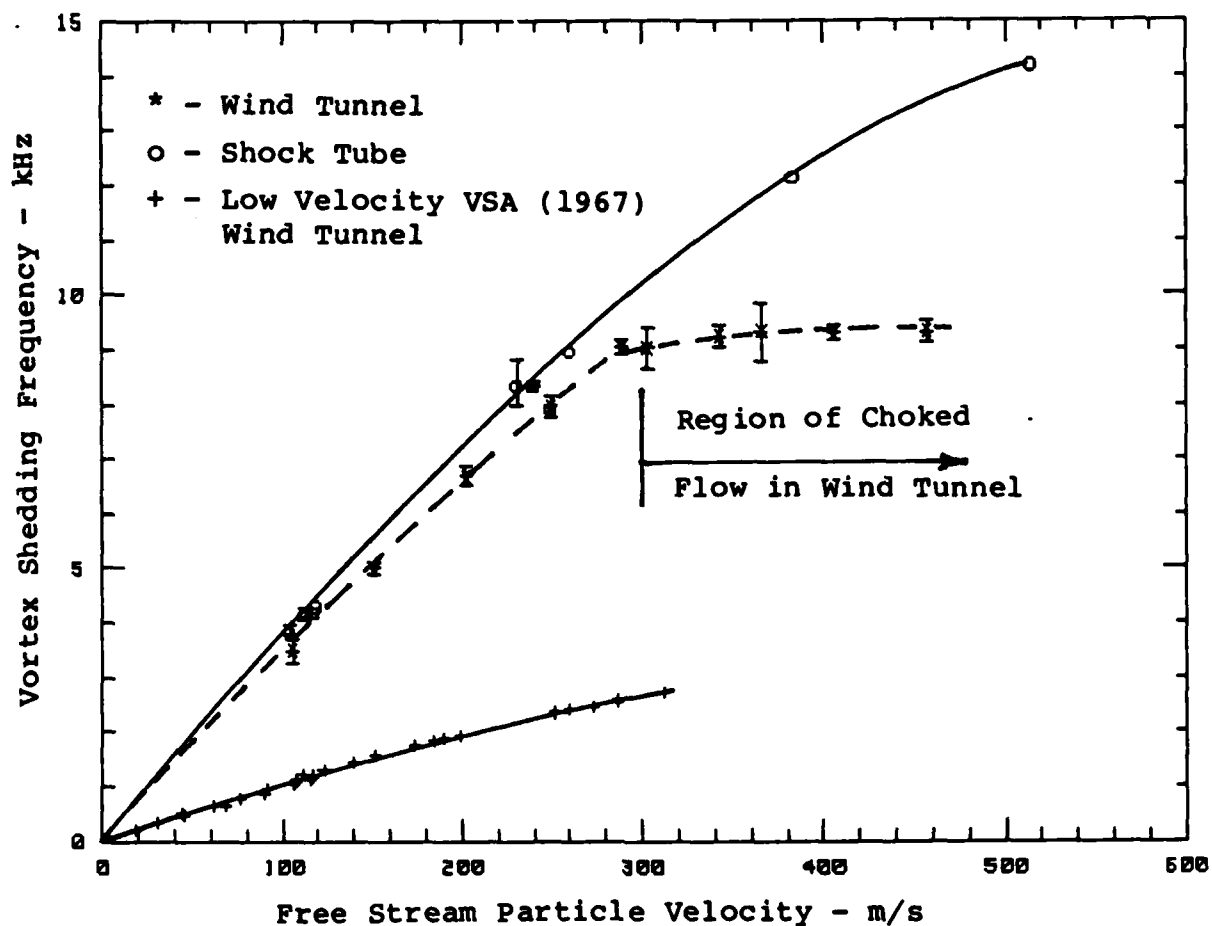
Figure 11.   Vortex shedding anemometer calibration.

Note the agreement between transient and steady-state flow calibration in the subsonic region below 300 m/s. The anomalous behavior of the HV-VSA in the supersonic flow is thought to be caused by choking in the flow channel during steady state conditions. The time required for the choking to develop depends on several factors but it is reasonable to expect that the transient shock tube measurement is made before the choking occurs.

Detailed results of both wind tunnel and shock tube calibrations are presented in Appendix A along with a discussion of interpretation of the raw VSA data and processing methods.

26

SECTION 4
FIELD TEST - DIRECT COURSE

This section presents a description of the HV-VSA application to measuring gas particle velocity in the air blast environment from event DIRECT COURSE.

4.1 EXPERIMENT DESCRIPTION

Objectives of experiment No. 7036 were to measure gas particle velocity time history during the positive flow phase from the air-blast wave, with comparisons between clean and dusty flow environments at various elevations. DIRECT COURSE provided an excellent test bed for evaluation of the newly developed high frequency version of the Vortex Shedding Anemometer (HV-VSA).

Three instruments were fielded along the Dusty South Radial and one along the Natural (clean) West Radial, all at the 600 ft ground range. The test matrix is given in Table 1. The expected peak overpressure of 240 kPa (35 psi) provided the first opportunity to observe the HV-VSA performance above Mach 1 in a non-ideal flow environment.

Table 1. Experiment No. 7036 test matrix.

Sensor Elevation (Inches)	South Radial (Dusty)	West Radial (Natural)
2	X	
6	X	X
12	X	

Ground Range 183 m (600 ft)

Predicted Peak Over Pressure 240 kPa (35 psi)

Predicted Peak Particle Velocity 335 m/s (1100 ft/s)

27

Figure 12 is a photograph showing the three channel mounting fixture installed along the dusty radial. Each HV-VSA is equipped with two subminiature pressure sensors that may be connected in a differential manner to cancel common mode overpressure effects. Due to the severe environment and high probability of physical damage to the delicate sensing elements, it was decided to record each channel independently. The gain of the right hand channel was setup at twice that of the corresponding left channel to enable one channel to capture the initial peak velocity while extending the range into the lower velocity region with the other.

BRL provided operational support for signal conditioning and data recording.

The transducer outputs were recorded using a constant bandwidth frequency multiplex (MUX) system that shared channels with other experiments. A one-line block diagram of the signal conditioning and recording system is shown in Figure 13.

4.2 FIELDING EXPERIENCES

Lessons learned while fielding the VSA on DIRECT COURSE are presented as guidance for others in order to avoid the same or similar problems on future test events. The situations and problems are generic in nature and not at all peculiar to the VSA measurement.

The first problem encountered relates to the installation of the VSA mounting hardware and field cable terminals. Figure 14 is a photograph showing details of the field installation. The first serious rain flooded the underground vault and shorted out the terminals. The obvious remedy for this situation was to seal the vault to be watertight. In this instance, silicone RTV sealant

28
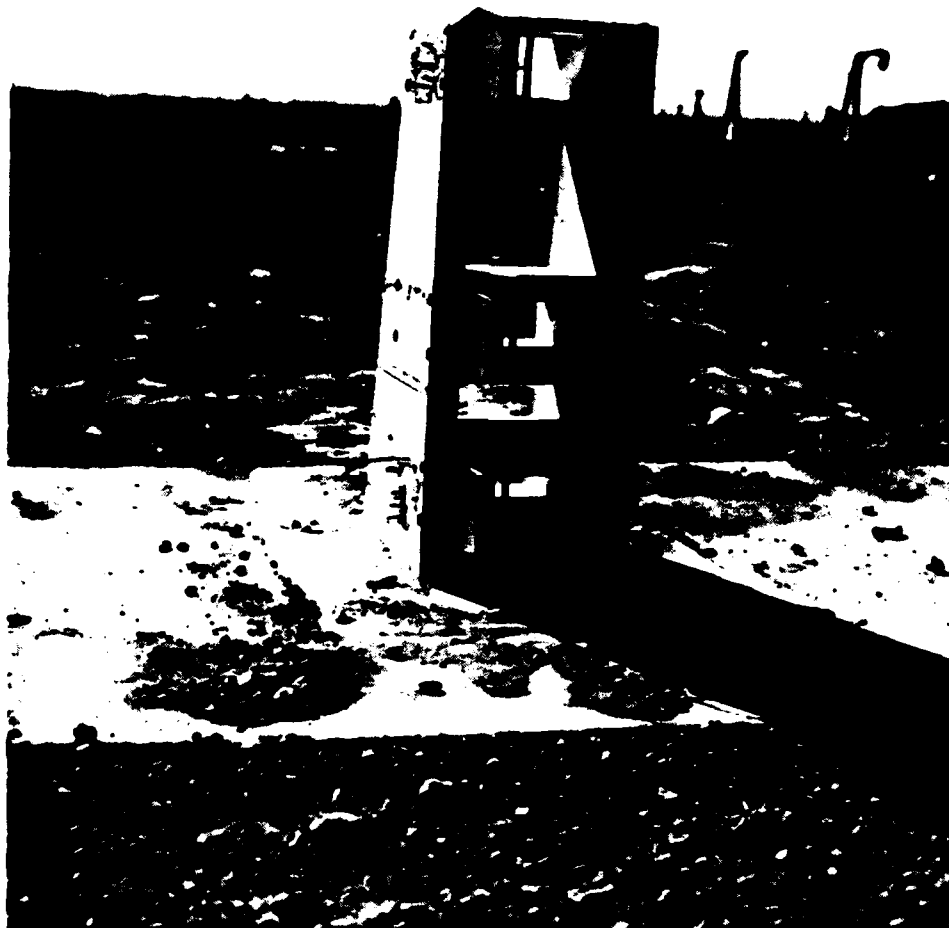
Figure 12.   Field installation of three channel
vortex shedding anemometer.

29

Data channel
Inputs
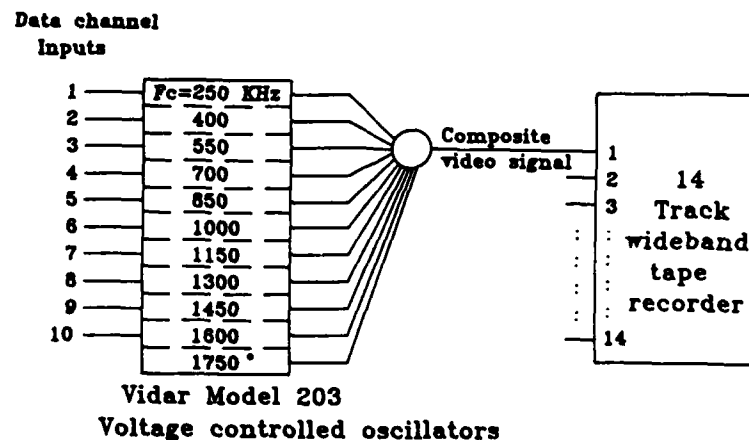
Data Recording System
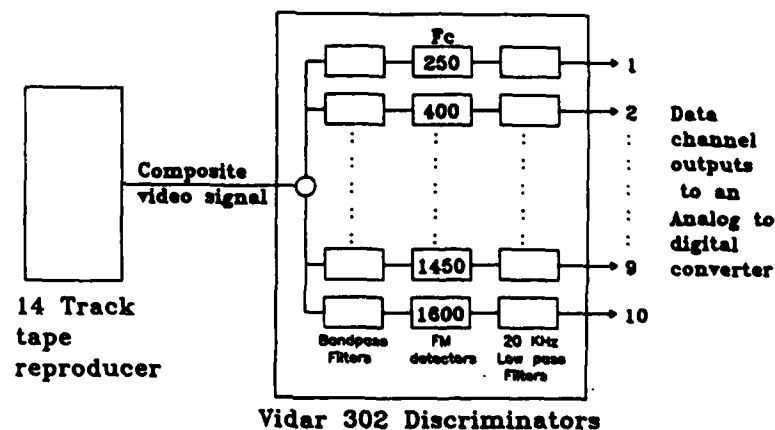
Data Playback System

Figure 13. Block diagram for DIRECT COURSE data
acquisition/reduction system.

Figure 14. VSA installation on dusty radial.

31

placed around the rim of the vault prior to installation of the VSA base plate provided the necessary seal. Additionally, the same material was used around the mounting bolts to seal against possible leak.

A second major problem was caused by a severe electrical storm. Induced voltages across the transducer elements destroyed or damaged all of the eight sensors. These were returned to the manufacturer for repair or replacement. During the interim, we reviewed the problem for preventative action to avoid a repeat performance. After exploring several possible alternatives, the transient suppressor 1N6041A was selected and installed across the transducer bridge elements.

The final lesson learned was much more subtle and potentially more damaging than the two related previously. It points up a problem in data acquisition that can result in data that is created by the recording system. The VSA channels were recorded on analog magnetic tape using a frequency multiplexed system to gain more effective utilization of the tape information storage capability.

The following section will present recorded results that appear to be VSA data but are in fact interference from an adjacent channel in the multiplex group.

4.3 MEASUREMENT RESULTS

Data were recorded on seven out of eight recording channels. A summary chart showing data return from all channels is given in Table 2. Observe that the data were recorded on the natural line for 22 milliseconds after the shock arrival and the dusty line measurement at the 5.1 cm elevation was lost after 11 milliseconds. The other two measurements extended until the signal diminished into the recording channel noise floor. The raw data records from these measurements are presented in Appendix B.

32

Table 2. VSA data summary.

Channel ID	ΔP_{max} (kPa)	Saturation Recovery (ms)	Gage Failure (ms)
Dusty Radial			
127-0-PS	300		
127-.17-VL(L)			11.1
127-.17-VL(R)			0
127-.5-VL(L)			
127-.5-VL(R)		19.1	35.8
127-1-VL(L)			
127-1-VL(R)		18.1	
Natural Radial			
227-0-PS	250		
227-.5-VL(L)			4.9
227-.5-VL(R)		13.0	22.2

4.4 DISCUSSION OF RESULTS

Detailed analysis of the recorded data revealed the presence of an interference signal superimposed on the data channels that started approximately 40 milliseconds prior to shock arrival at the VSA location. Unfortunately, the spectral content of the noise is in the same frequency range as the expected data and the two signals are inextricably mixed together. Upon further exploration, the source of noise was determined to be from interchannel modulation in the MUX system. We learned that the Field Sciences Laboratory at KSC had encountered this same problem ten years

33

earlier on underground test event DINING CAR. Appendix C is a
copy of a paper on this topic that was presented at the DNA DINING
CAR Instrumentation Review meeting, July 1975.

An example of the interference introduced by the recording
system is presented in Figure 15 which shows an unidentified data
record along with the VSA data from channel 127-1-VL-L. Both of
these signals (and others) were multiplexed in the same system
before recording on a single track of the analog instrumentation
tape. Figure 16 shows the spectral content of the VSA channel
starting at 50 milliseconds prior to air shock arrival at the
600 ft station where the VSA was located. The VSA channel clearly
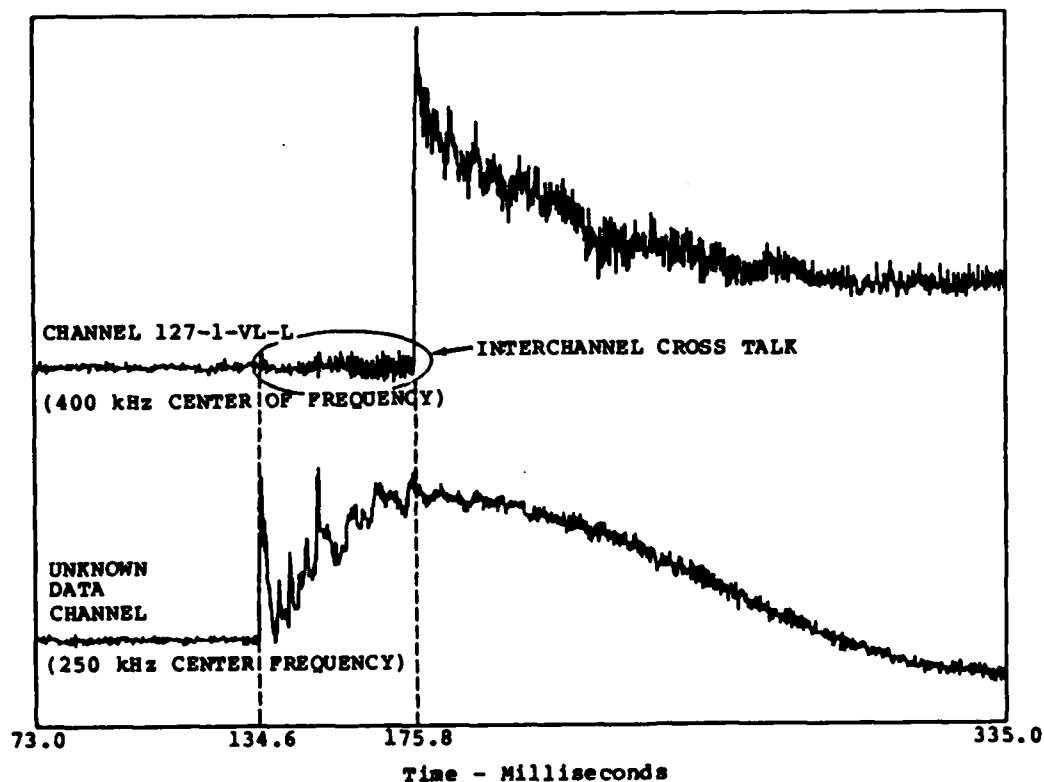shows the influence of the signal from the adjacent multiplex
channel.

CHANNEL 127-1-VL-L

INTERCHANNEL CROSS TALK

(400 kHz CENTER OF FREQUENCY)

UNKNOWN
DATA
CHANNEL

(250 kHz CENTER FREQUENCY)

73.0   134.6   175.8   335.0

Time - Milliseconds
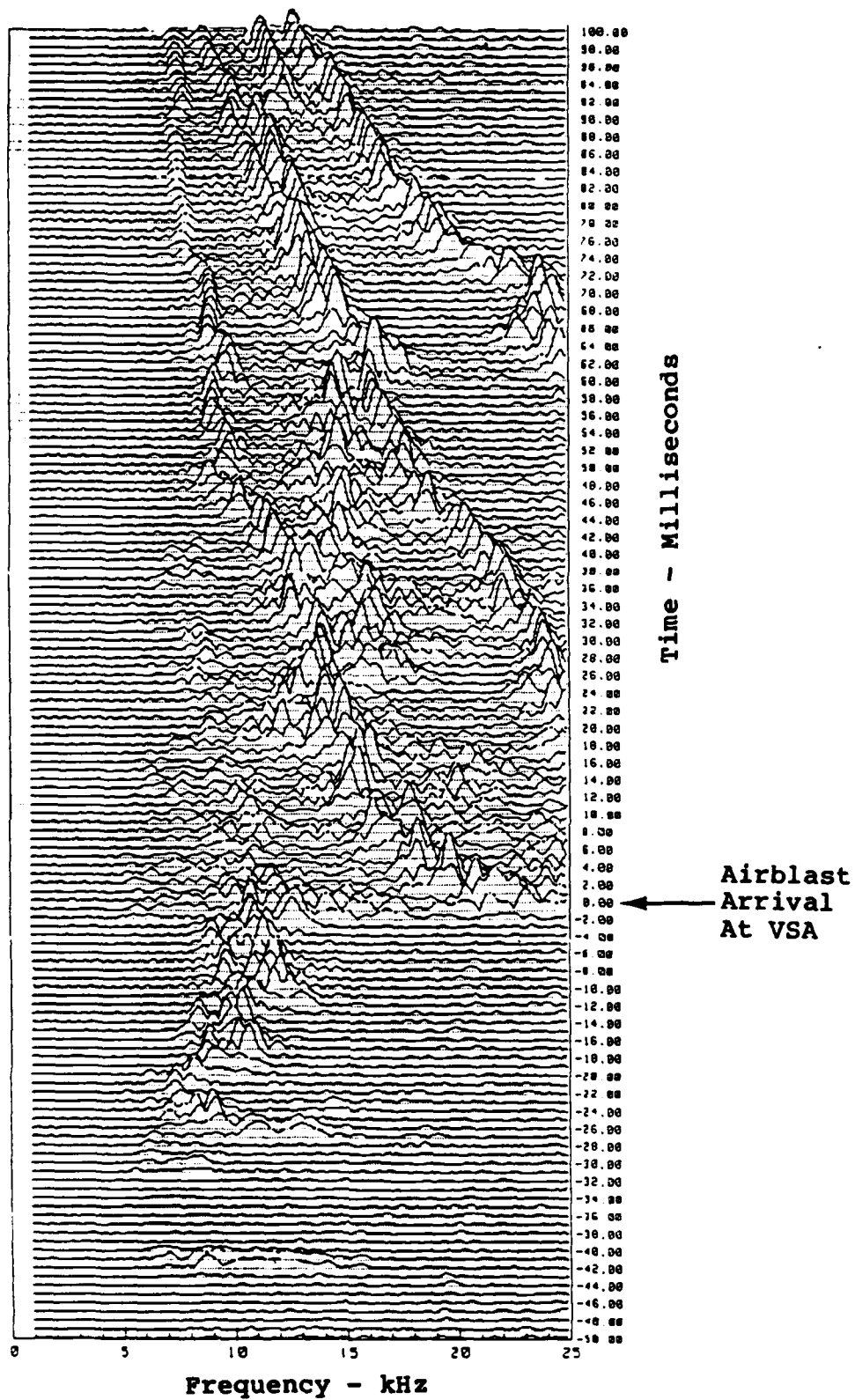
Figure 15. Multiplex cross talk.

34

Figure 16. Stack plot of frequency spectra for
Channel 127-1-VL-L (2 ms windows).

This level of interference is judged to be unacceptable for unambiguous interpretation of the VSA data since the spectral content of the interference is within the data band of the VSA and interpretation of the VSA data is frequency dependent.

Presence of the interference signal prior to shock arrival at the VSA stations clearly identifies the problem. However, there is no reason to believe that the VSA channels did not contaminate each other's data also. This is especially probable for the right gage channel, which was deliberately set to saturate during early time in order to extend the low end of the measurement.

For comparison with Figure 16 and as an example of the expected signal, Figure 17 shows the HV-VSA output signal response and spectral content of a shock tube calibration shot of the HV-VSA at a peak flow velocity of 230 m/s (755 ft/s). Reduced data from this shot given in Figure 18 shows the flow velocity versus time.

A complete set of data from experiment 7036 is included in Appendix B.
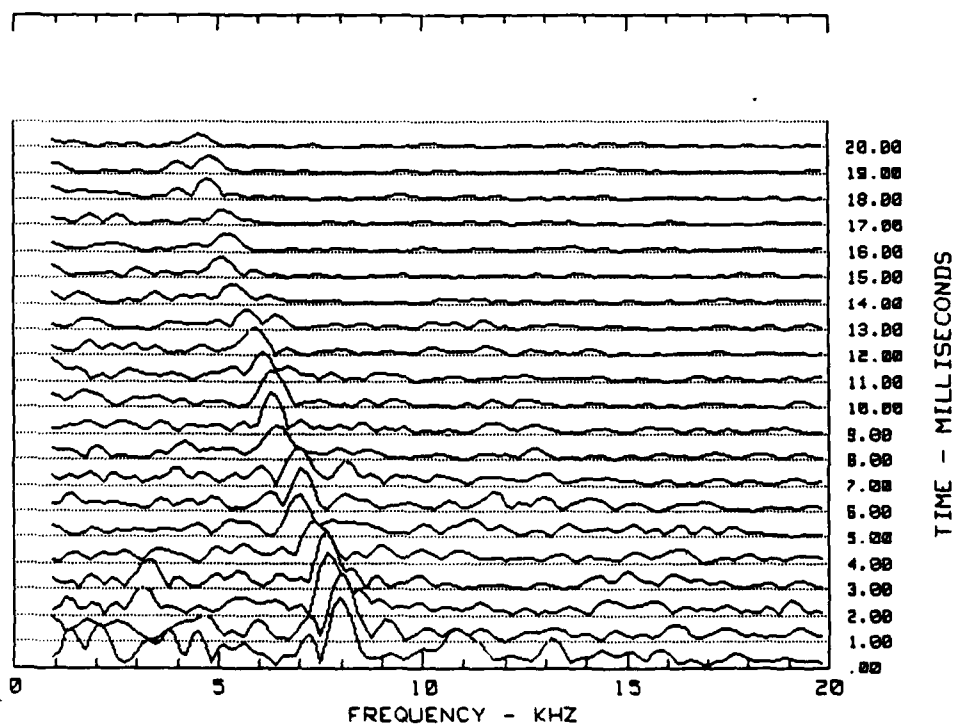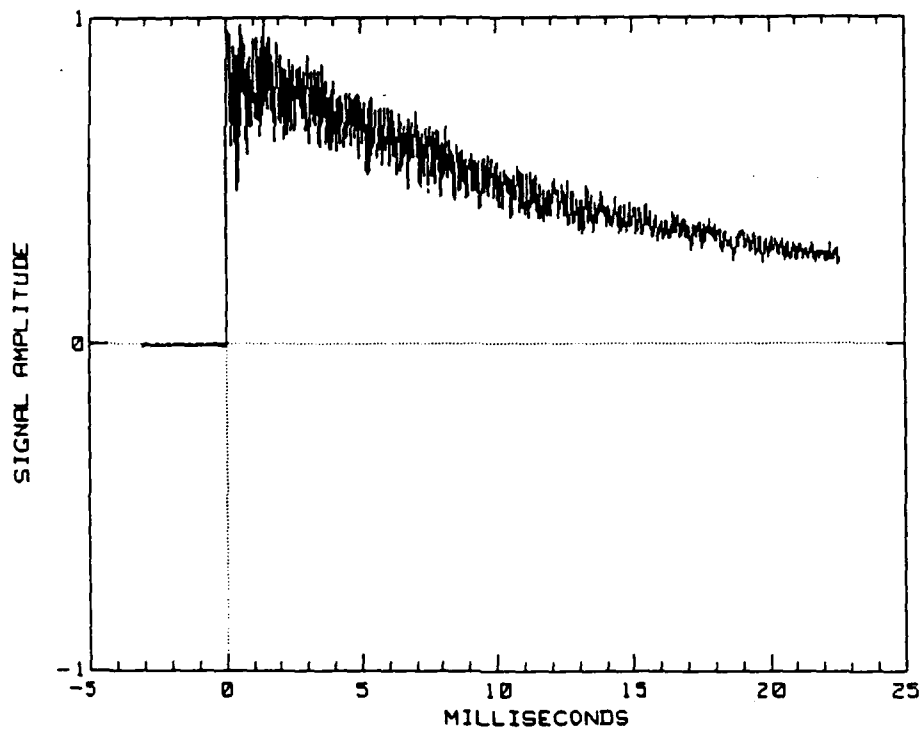
36

Figure 17. Typical HV-VSA response to shock tube.
Test conditions: Overpressure = 53.8 kPa,
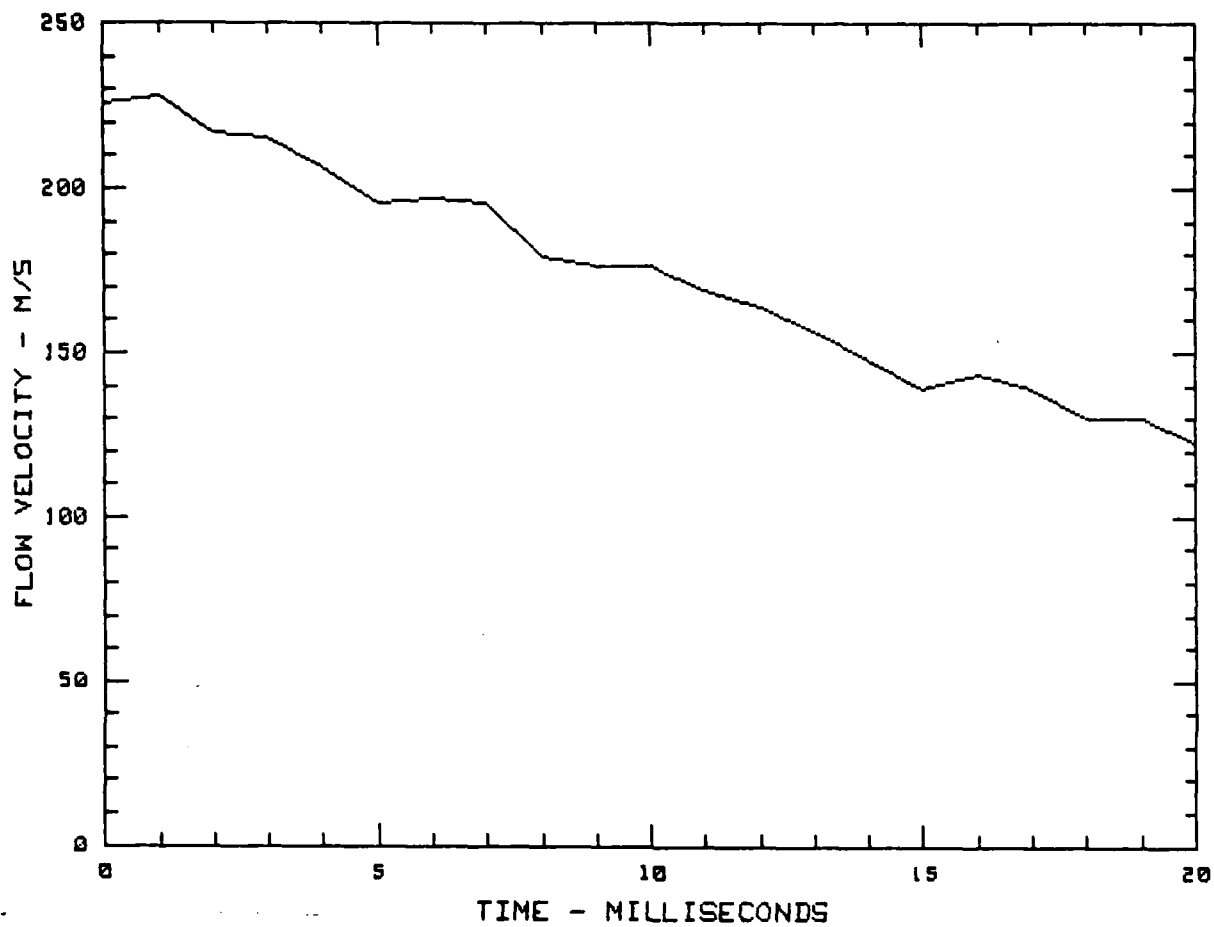Velocity = 250 m/s.

37

BRL Shot 8

Figure 18. Measured shock tube particle velocity profile.

SECTION 5
CONCLUSIONS AND RECOMMENDATIONS

The HV-VSA with its smaller diameter vortex generator has been demonstrated to operate well into the supersonic flow regime. Placement of the pressure sensing ports was found to be more critical (in absolute terms) and the HV-VSA output waveform was observed to be much more complex, making simple analysis of the measurement data no longer feasible.

Tradeoffs between the HV- and LV-VSA are tabulated in Table 3 showing relative merit of each model.

Table 3. Comparison of HV-VSA versus LV-VSA.

	LV-VSA	HV-VSA
Vortex Generator Diameter (mm)	16.9	4.2
Calibration Limit (m/s)	310	515*
Shedding Frequency at Cal Limit (kHz)	2.7	14.2
Output Waveform	Sinusoidal	Complex
Port Orientation	Cross-Stream	Upstream
Relative Ruggedness	More	Less

* Limitation imposed by shock tube facility.

The LV-VSA should be preferred for measurements in the extremely hostile environment of the boundary layer flow conditions from a large-charge high explosives test such as DIRECT COURSE. This recommendation is based on observed posttest damage caused by dust and debris impact on the relatively more fragile sensing element of the HV-VSA.

39

Field experiences have emphasized the need for very careful consideration of pretest protection against natural elements of the environment. It is not necessarily prudent to assume that weatherproof housings are adequate for protection against water invasion even though the desert is envisioned to have a dry climate. Also, attention is directed toward the need for adequate protection against lightning induced voltages that may damage sensitive transducer sensing elements and signal conditioning electronics.

The Vidar Multiplex System in DNA's inventory of field instrumentation is a valuable and effective means of adding additional recording channels to an instrumentation tape recorder but its limitations and potential pitfalls require careful consideration by the experimenter as well as the recording station operations personnel.

The difficulties experienced with the multiplexed signals were not observed during calibration of the VSA in either wind tunnel or shock tube tests where channel-per-track recording techniques were used.

In summary, two versions of the VSA have been tested in the steady flow field from a wind tunnel and in the transient flow environment of a gas driven shock tube. For supersonic flow, the wind tunnel data indicated choked flow through the vortex generating and sensing channel. The HV-VSA performed very well and was also calibrated in the transient flow in a gas-driven shock tube. The velocity limit of the facility was extended up to a shock Mach 2.2 with a helium driver to achieve a maximum flow velocity of 510 m/s.

The subject of choked flow in the VSA requires further study and consideration for further development of the instrument for application to supersonic velocity measurements.

REFERENCES

1. Baker, Wilfred E., "Explosions in Air," University of Texas
    Press, Austin and London, 1973, p 30.

2. Dewey, John M., "The Air Velocity and Density in Blast Waves
    from TNT Explosions," Suffield Report No. 207, Defence
    Research Establishment Suffield, Ralston, Alberta, Canada,
    March 1964.

3. Funk, John W., David H. Saint, "A System for Measuring Total
    Density in Dusty Shock Waves Using the Beta Attenuation
    Technique," Proceedings of the 30th International Instrumen-
    tation Symposium, 1984, p 663.

4. "Development of Air Blast Instrumentation: Vortex Shedding
    Anemometer and High-G Accelerometer," DASA 2334, March 1969.

5. Sachs, D. C., "Field Test Particle Velocity Gage, Operation
    DISTANT PLAIN Symposium, Volume II," M. J. Dudash, Editor,
    DASA 2207, May 1968.

6. Joy, Robert D., "Ultrasonic Vortex Flowmeters," Proceedings
    of the 30th International Instrumentation Symposium, 1984,
    p 224.

42

APPENDIX A

VSA CALIBRATION

The High Velocity Vortex Shedding Anemometer (HV-VSA) was calibrated both in the trisonic wind tunnel facility at the United States Air Force Academy (USAFA), Colorado and in the 0.61 meter (24 inch) shock tube at Ballistic Research Laboratories, Aberdeen, Maryland. Raw data and spectral stack-plots are presented in this appendix.

A-1 WIND TUNNEL TESTS

The USAFA Trisonic Tunnel is a 30.5 cm square blowdown facility in which compressed air exhausts to the atmosphere. A porous wall transonic test section provides variable Mach numbers between 0.31 and 1.2. Fixed nozzle blocks are available for Mach numbers of 1.40, 1.67, 3.48 and 4.38.

The HV-VSA was sting mounted in the test section and a series of calibration runs at various Mach numbers was completed. The calibration matrix is shown in Table A-1. The VSA output signals were recorded on a 20 kHz analog tape recorder for later data reduction and analysis. Tunnel diagnostics were provided to KSC by the wind tunnel operations personnel. Typically, steady flow conditions were established in 10 to 20 seconds of blowdown.

Data reduction procedure was to sample several portions of the signal at various times during the test. These data were then analyzed using Fast Fourier transforms to display the spectral content at regularly spaced intervals. Deviation of the frequency

43

Table A-1. Wind tunnel calibration.

Mach No.	Velocity (m/s)	Frequency (kHz)	Run No.
.31	105.46	3.45	2
.45	151.18	5.00	3
.61	201.78	6.69	4
.77	249.33	7.96	5
.91	288.65	9.03	6
.97	302.67	9.03	7
1.13	342.29	9.28	8
1.23	365.76	9.31	9
1.40	405.38	9.30	17
1.67	456.90	9.32	18

from the mean could be either fluctuations in flow velocity or response variations of the VSA. We expect the former to be true but have no standard reference for comparison to validate the hypothesis.

Raw data and spectral stack plots from the wind tunnel calibration runs are given in Figures A-1 through A-10.

A-2 SHOCK TUBE TESTS

The HV-VSA was tested in the transient air flow field of the 0.61 meter shock tube at the USA Ballistic Research Laboratories (BRL), Aberdeen Proving Ground, Maryland. A total of ten shots were fired at nine discrete velocities. Test conditions and measured VSA frequency output are presented in Table A-2. Notice that on some of the tests, a partial vacuum was pumped on the pipe driven section; some tests had the driven pipe at atmospheric pressure and for the highest velocity attained, the driver gas was helium and partial vacuum was pumped on the driven pipe section.

Table A-2. Shock tube calibration.

$\dfrac{P}{P_o}$	Velocity (m/s)	Frequency (kHz)	Gas Driver	Shot No.
0.51	103.94	3.88	Air	2
0.56	112.47	4.18	Air	1
0.59	117.65	4.25	Air	10
0.59	118.26	4.35	Air	7
1.41	230.73	8.40	Air	4
1.47	239.57	8.38	Air	3
1.56	249.63	7.95	Air	8
1.66	260.30	9.00	Air	9
2.95	383.13	12.20	Air	5
4.75	514.81	14.25	He	6

Data acquisition was via channel-per-track wideband Group I analog instrumentation magnetic tape recorder. As with the wind tunnel tests, the shock tube diagnostics were furnished by BRL and the VSA data reduction was performed at KSC. Flow velocity taken as the value immediately behind the shock was used to correlate with a frequency of the VSA response.

Raw data from these tests are presented in Figures A-11 through A-20 along with spectral plots of the VSA data signal. Data from Shot 8 has been selected as a typical example of a VSA measurement application. In a somewhat self-calibrating mode, the VSA has measured the variation in flow velocity behind the shock front. Frequencies selected from the spectral stack plot in Figure A-18 have been translated into velocities via the calibration curve (Figure A-21). The flow velocity time history for Shot 8 as indicated by the VSA is given in Figure A-22. This example was chosen because the wave was peaked and illustrates the dynamic capabilities of the instrument.

45

MAXIMUM FREQUENCY= 50 KHZ
FREQUENCY RESOLUTION= 90 HZ
TIME WINDOW= 2 MILLISEC
NUMBER OF TIME POINTS= 1024
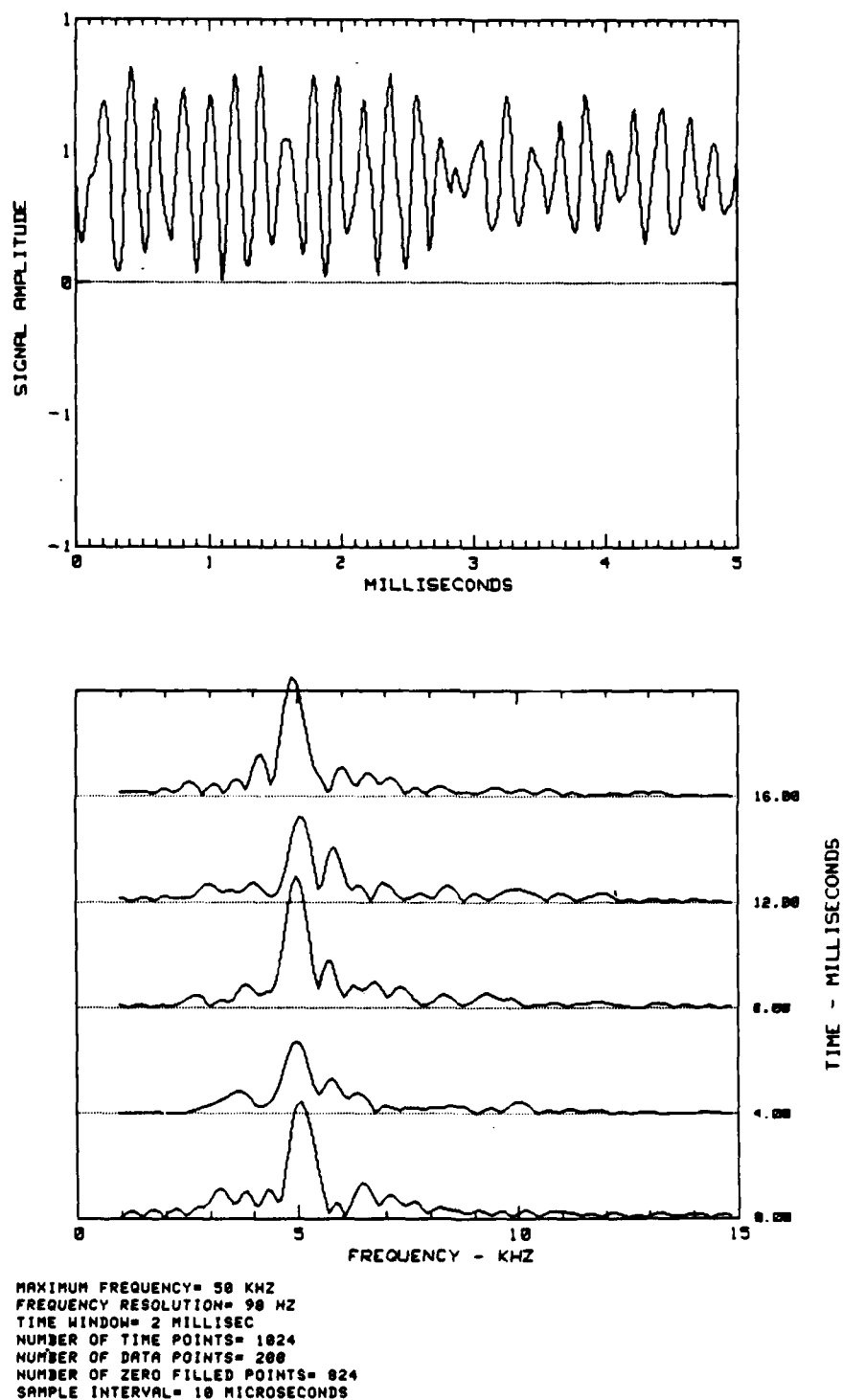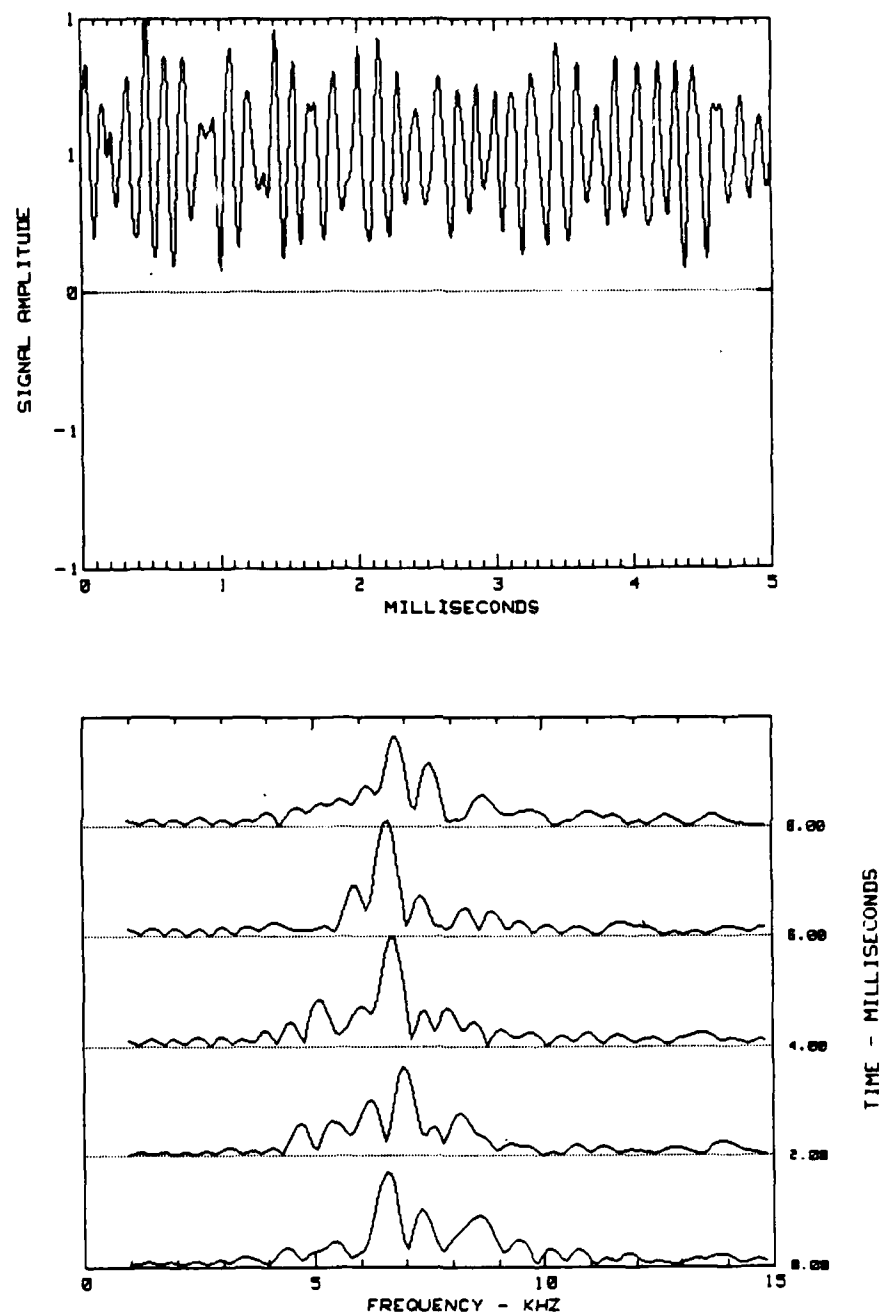NUMBER OF DATA POINTS= 200
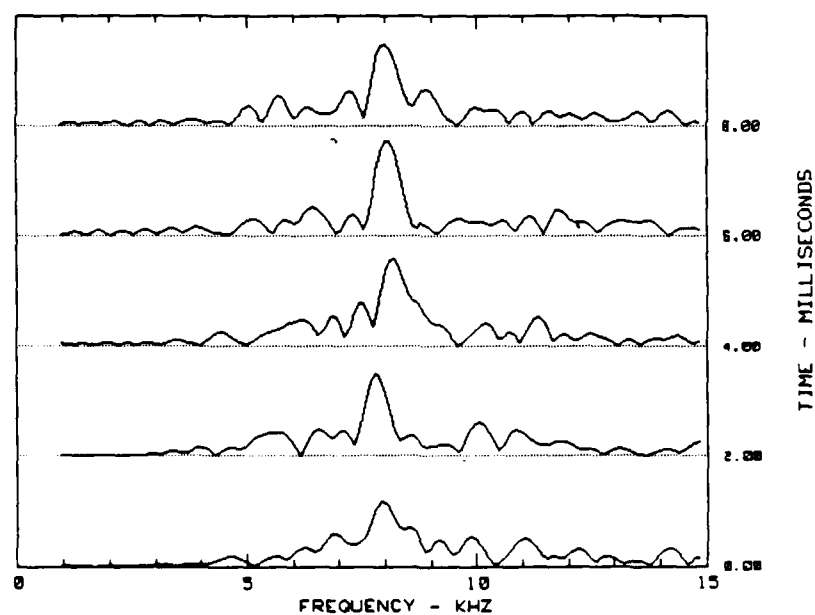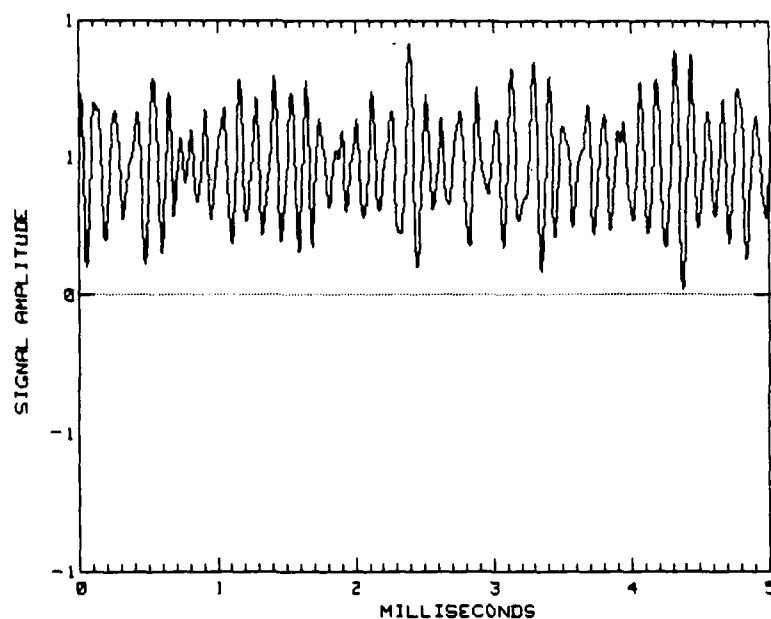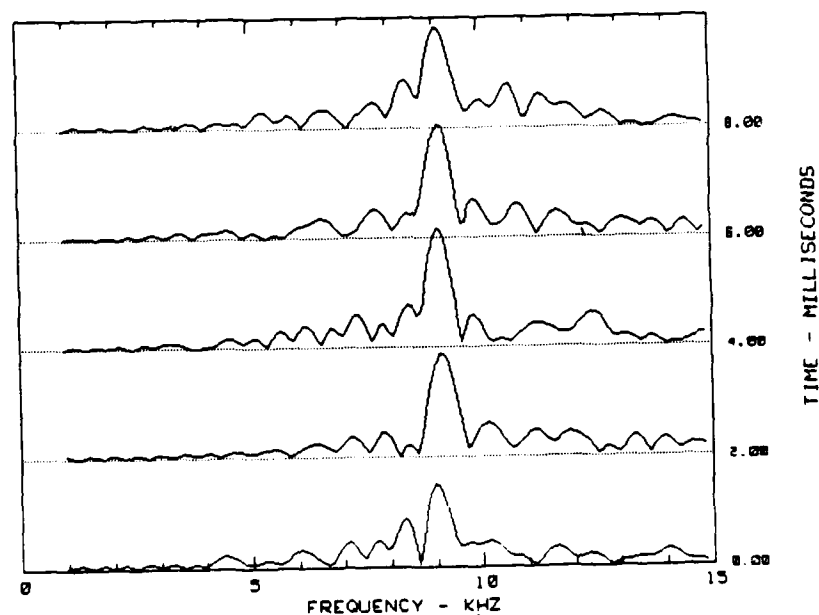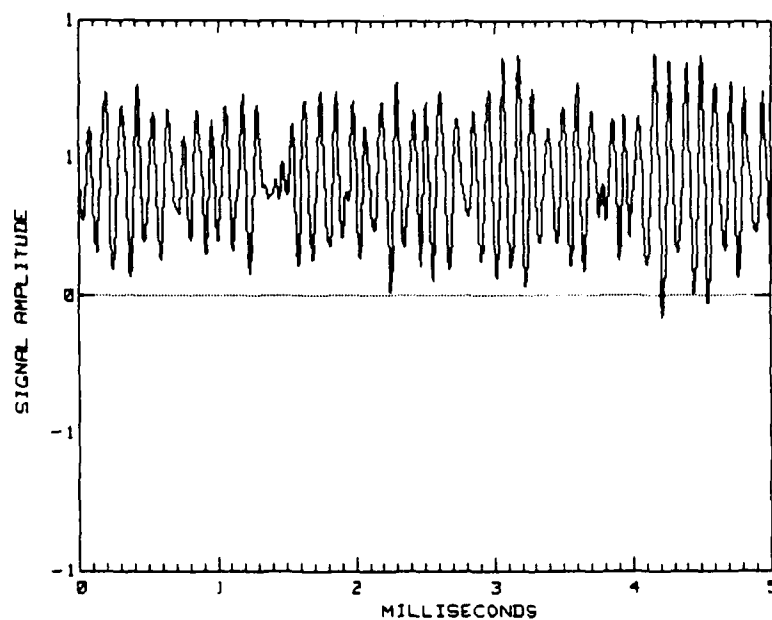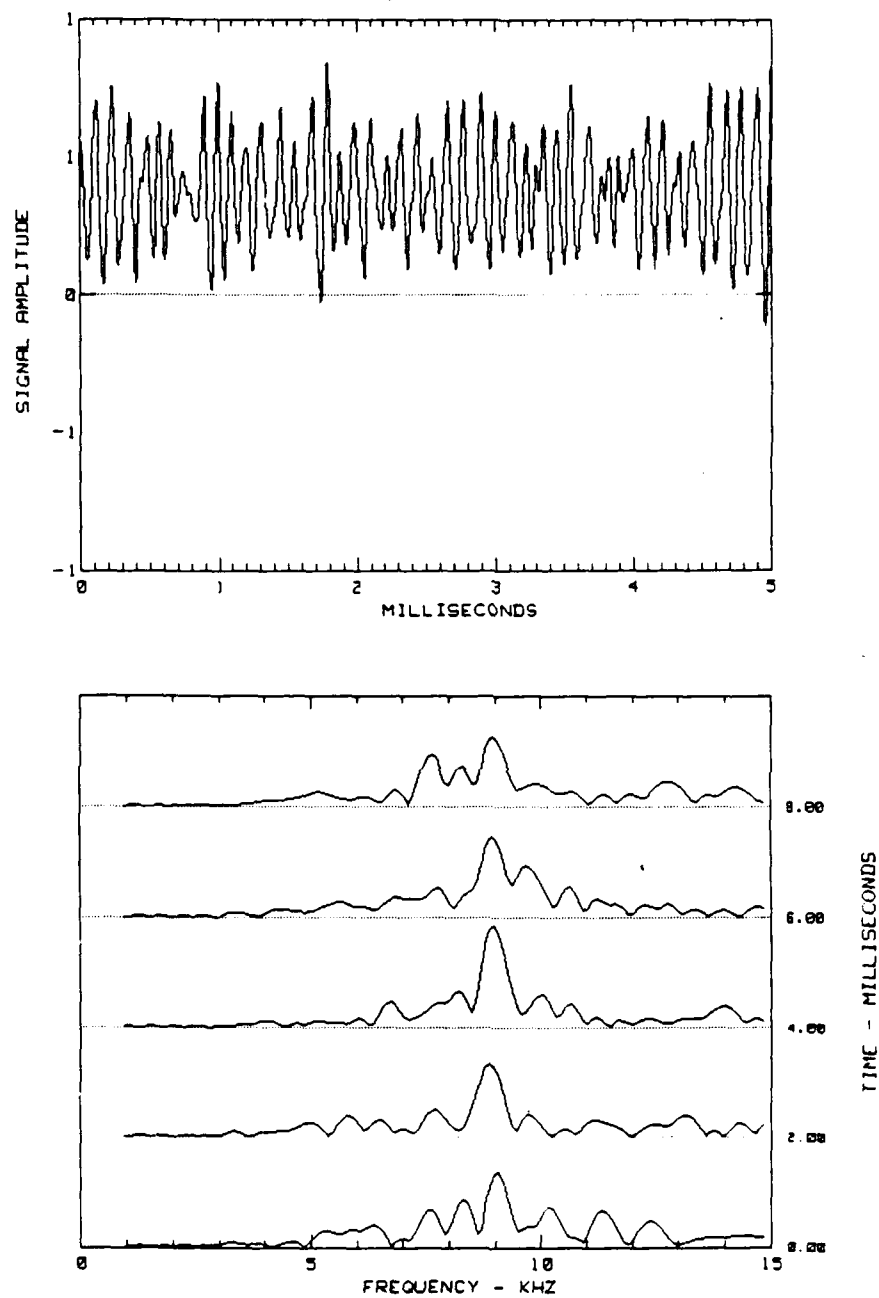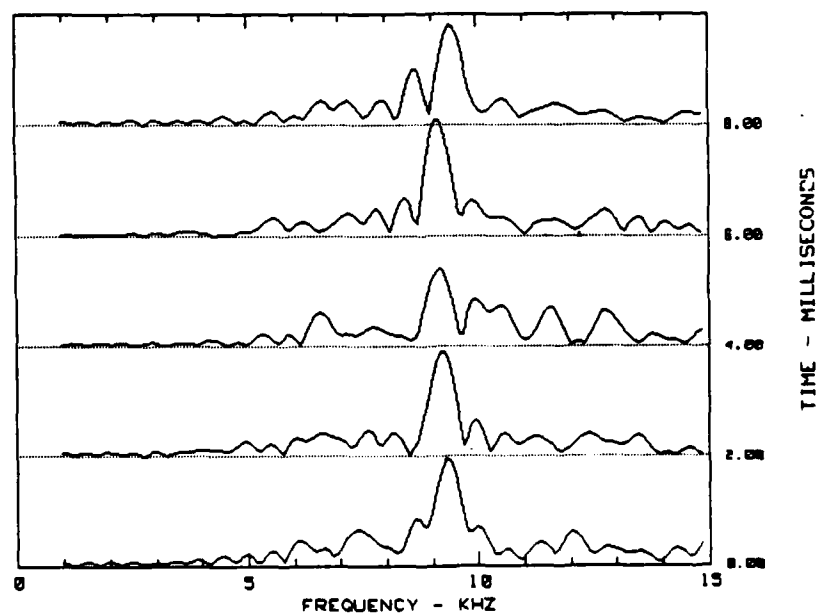NUMBER OF ZERO FILLED POINTS= 824
SAMPLE INTERVAL= 10 MICROSECONDS
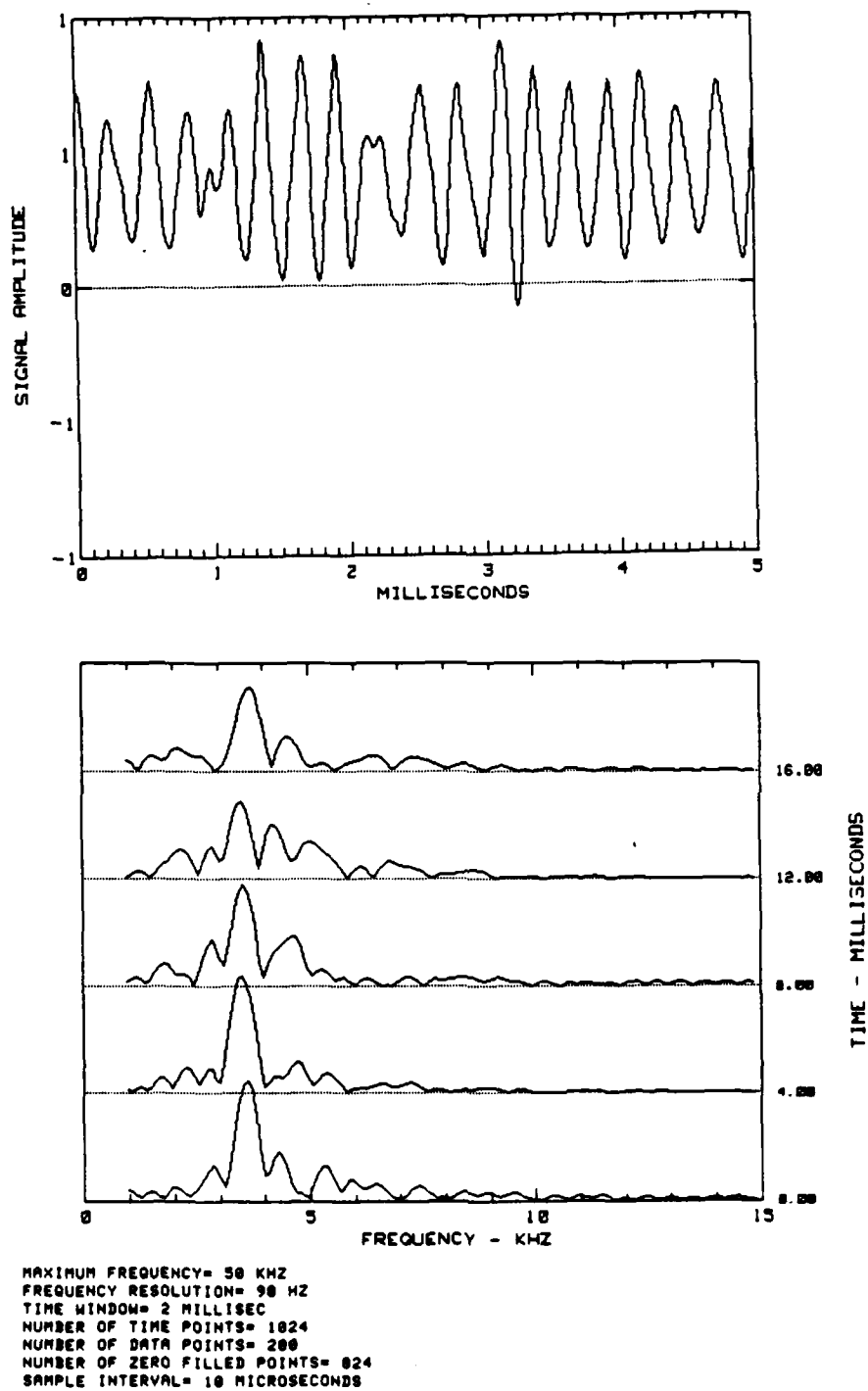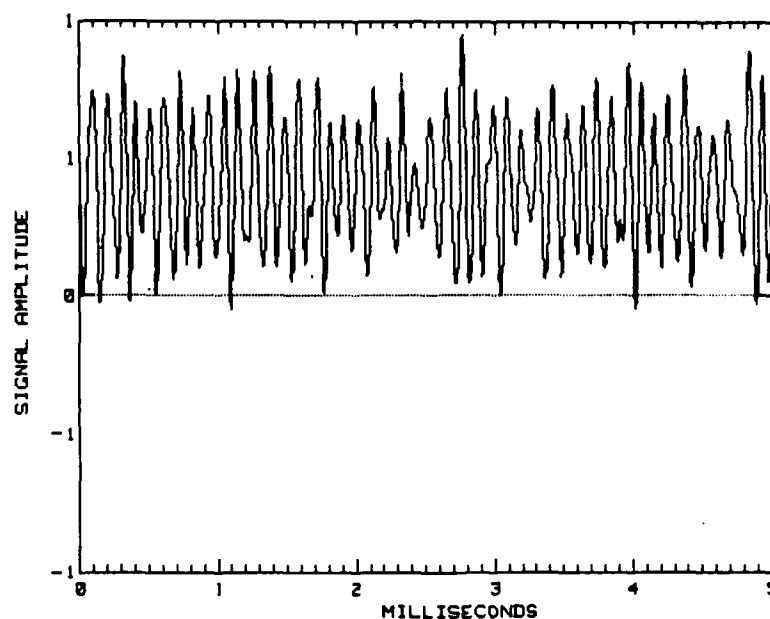
Figure A-1. HV-VSA calibration (M = 0.31).

46

MAXIMUM FREQUENCY= 50 KHZ
FREQUENCY RESOLUTION= 98 HZ
TIME WINDOW= 2 MILLISEC
NUMBER OF TIME POINTS= 1024
NUMBER OF DATA POINTS= 200
NUMBER OF ZERO FILLED POINTS= 824
SAMPLE INTERVAL= 10 MICROSECONDS

Figure A-2. HV-VSA calibration (M = 0.45).

47

MAXIMUM FREQUENCY= 100 KHZ
FREQUENCY RESOLUTION= 98 HZ
TIME WINDOW= 2 MILLISEC
NUMBER OF TIME POINTS= 2048
NUMBER OF DATA POINTS= 400
NUMBER OF ZERO FILLED POINTS= 1648
SAMPLE INTERVAL= 5 MICROSECONDS

Figure A-3.   HV-VSA calibration (M = 0.61).

MAXIMUM FREQUENCY= 100 KHZ
FREQUENCY RESOLUTION= 98 HZ
TIME WINDOW= 2 MILLISEC
NUMBER OF TIME POINTS= 2048
NUMBER OF DATA POINTS= 400
NUMBER OF ZERO FILLED POINTS= 1648
SAMPLE INTERVAL= 5 MICROSECONDS

Figure A-4. HV-VSA calibration (M = 0.77).

49

MAXIMUM FREQUENCY= 100 KHZ
FREQUENCY RESOLUTION= 98 HZ
TIME WINDOW= 2 MILLISEC
NUMBER OF TIME POINTS= 2048
NUMBER OF DATA POINTS= 400
NUMBER OF ZERO FILLED POINTS= 1648
SAMPLE INTERVAL= 5 MICROSECONDS
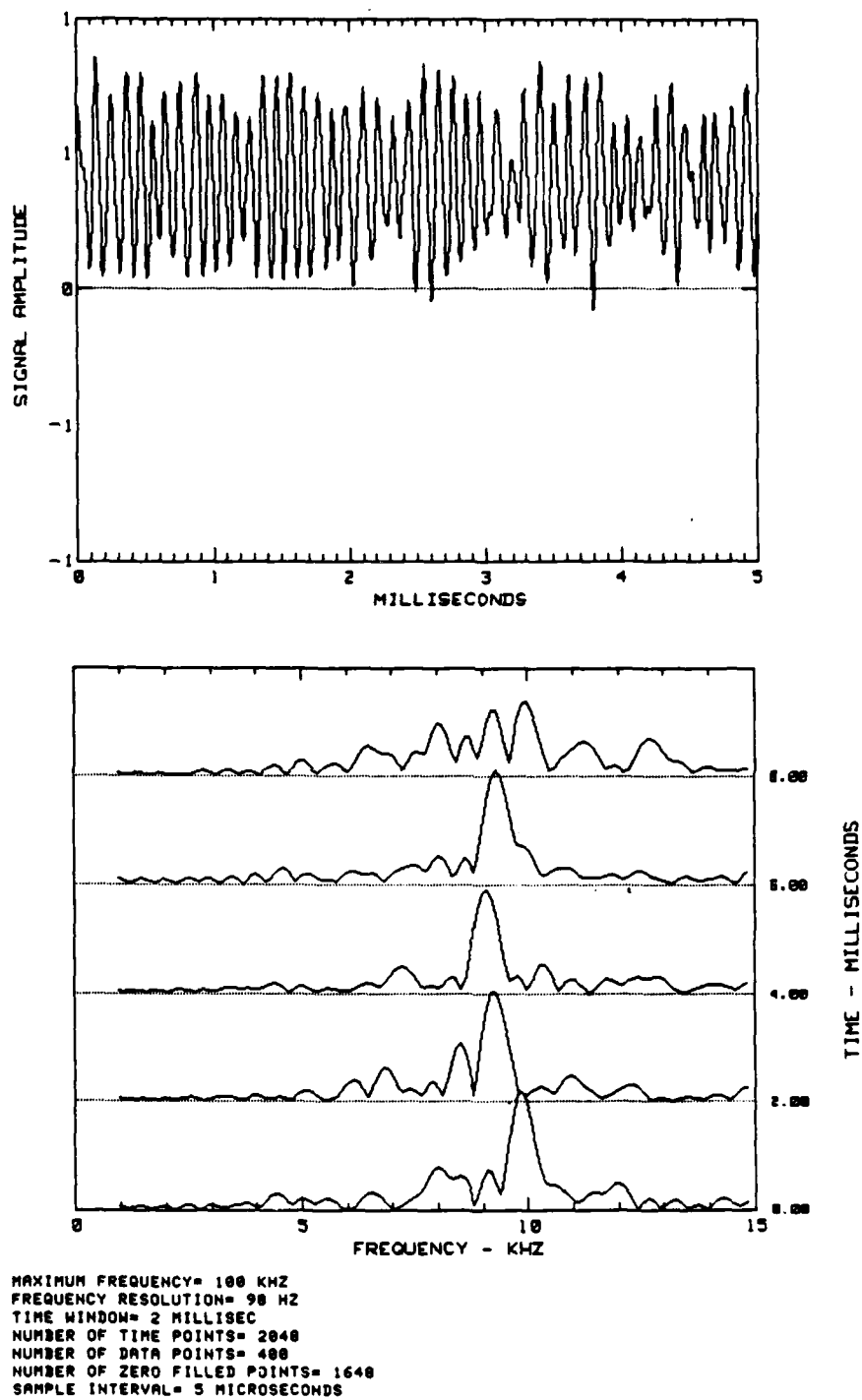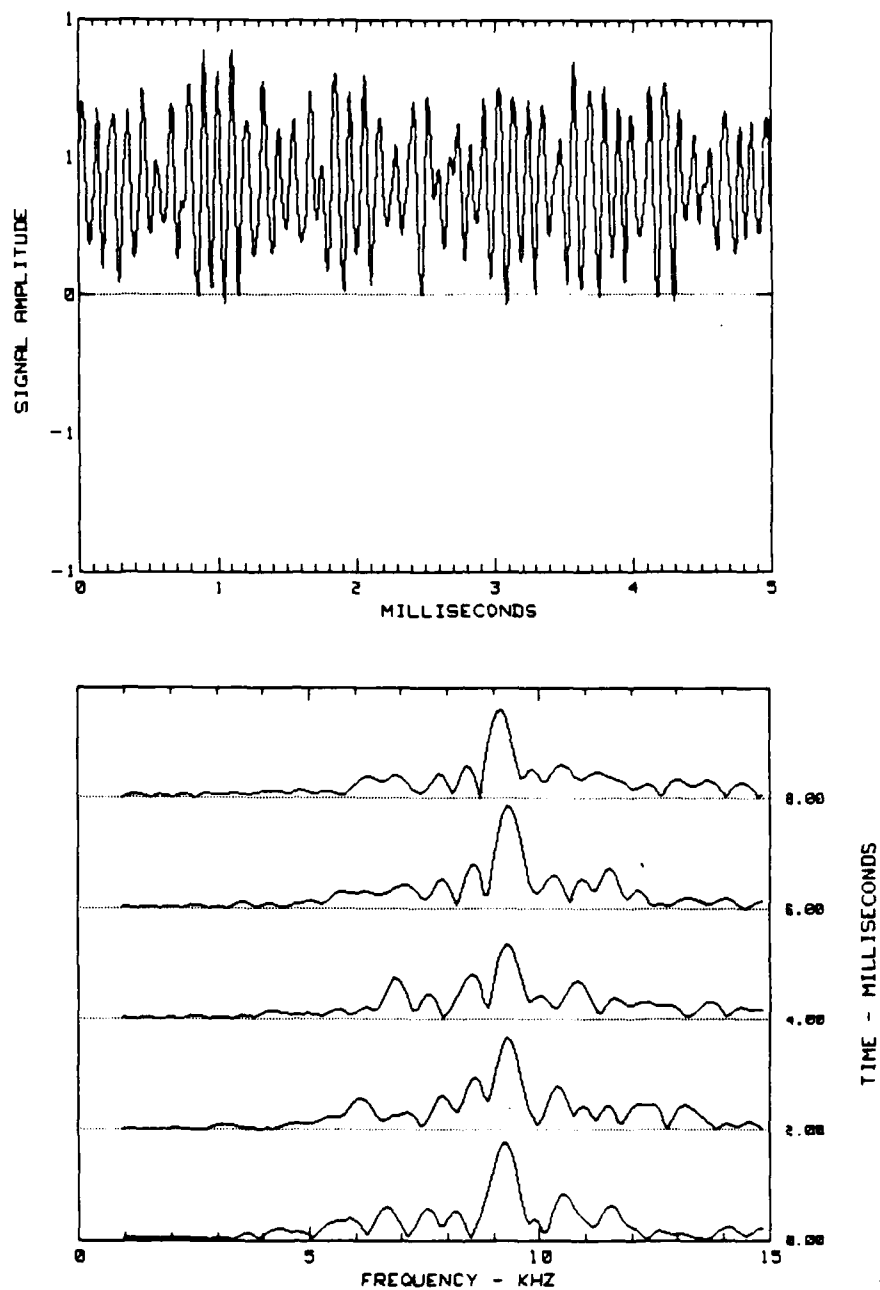
Figure A-5. HV-VSA calibration (M = 0.91).

50

MAXIMUM FREQUENCY= 100 KHZ
FREQUENCY RESOLUTION= 98 HZ
TIME WINDOW= 2 MILLISEC
NUMBER OF TIME POINTS= 2048
NUMBER OF DATA POINTS= 400
NUMBER OF ZERO FILLED POINTS= 1648
SAMPLE INTERVAL= 5 MICROSECONDS
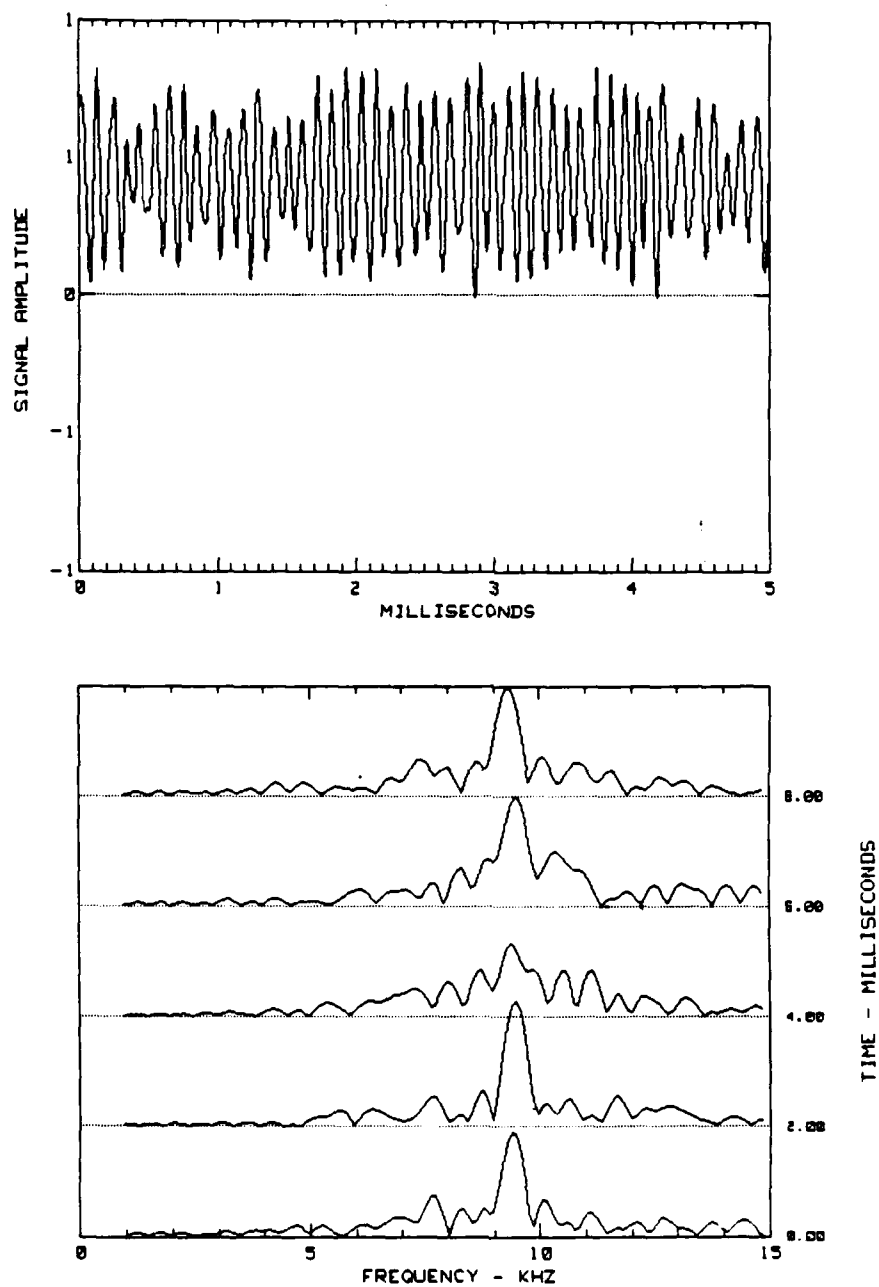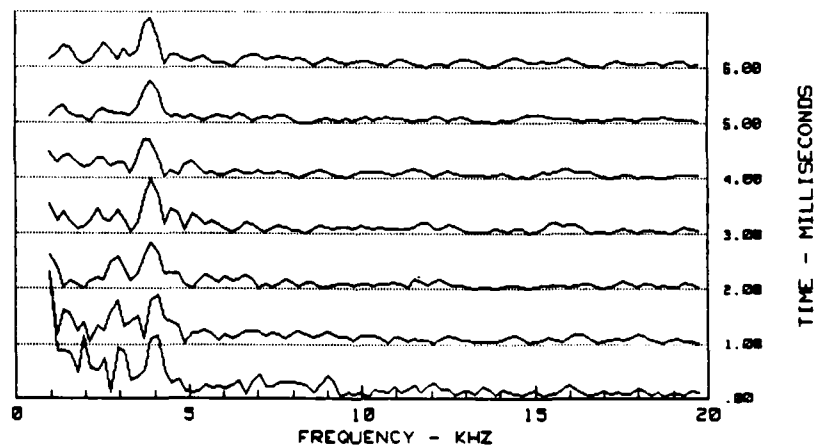
Figure A-6.   HV-VSA calibration (M = 0.97).

51

MAXIMUM FREQUENCY= 100 KHZ
FREQUENCY RESOLUTION= 98 HZ
TIME WINDOW= 2 MILLISEC
NUMBER OF TIME POINTS= 2048
NUMBER OF DATA POINTS= 400
NUMBER OF ZERO FILLED POINTS= 1648
SAMPLE INTERVAL= 5 MICROSECONDS
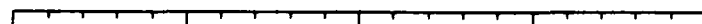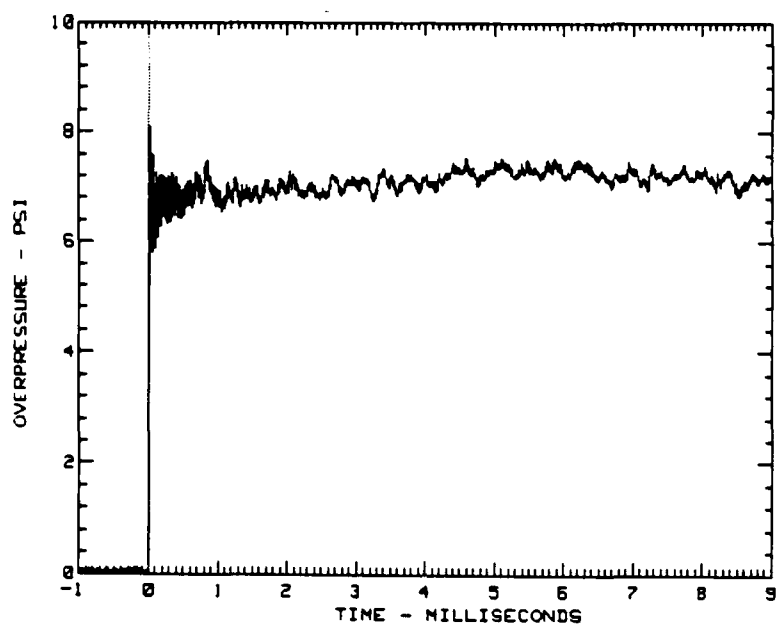
Figure A-7.   HV-VSA calibration (M = 1.13).

MAXIMUM FREQUENCY= 100 KHZ
FREQUENCY RESOLUTION= 98 HZ
TIME WINDOW= 2 MILLISEC
NUMBER OF TIME POINTS= 2048
NUMBER OF DATA POINTS= 400
NUMBER OF ZERO FILLED POINTS= 1648
SAMPLE INTERVAL= 5 MICROSECONDS

Figure A-8.   HV-VSA calibration (M = 1.23).

53

MAXIMUM FREQUENCY= 100 KHZ
FREQUENCY RESOLUTION= 98 HZ
TIME WINDOW= 2 MILLISEC
NUMBER OF TIME POINTS= 2048
NUMBER OF DATA POINTS= 400
NUMBER OF ZERO FILLED POINTS= 1648
SAMPLE INTERVAL= 5 MICROSECONDS
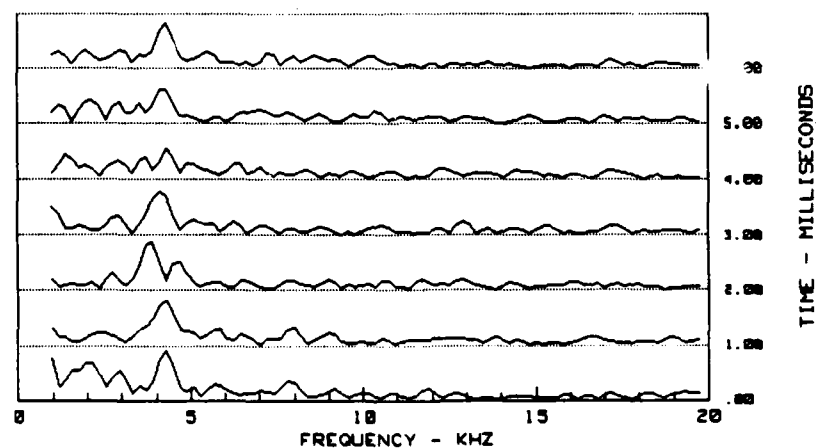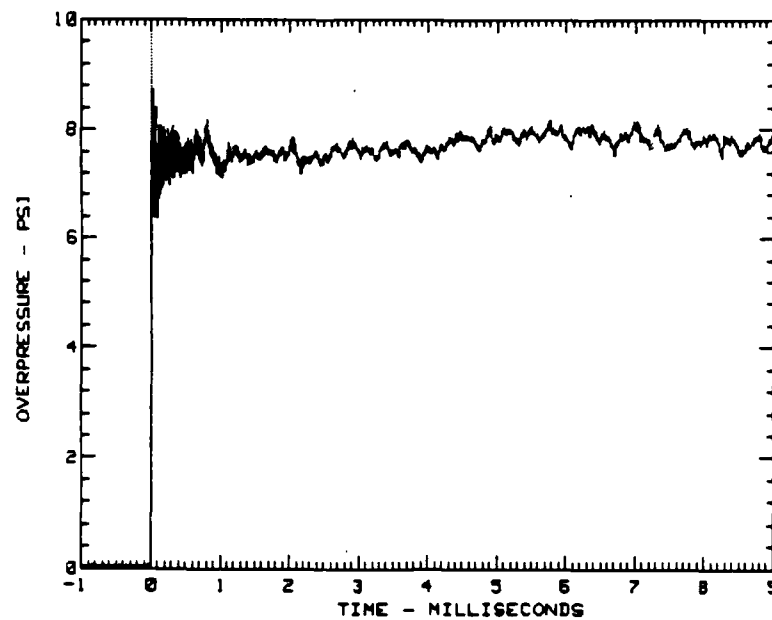
Figure A-9.   HV-VSA calibration (M = 1.40).

54

MAXIMUM FREQUENCY= 100 KHZ
FREQUENCY RESOLUTION= 98 HZ
TIME WINDOW= 2 MILLISEC
NUMBER OF TIME POINTS= 2048
NUMBER OF DATA POINTS= 400
NUMBER OF ZERO FILLED POINTS= 1648
SAMPLE INTERVAL= 5 MICROSECONDS
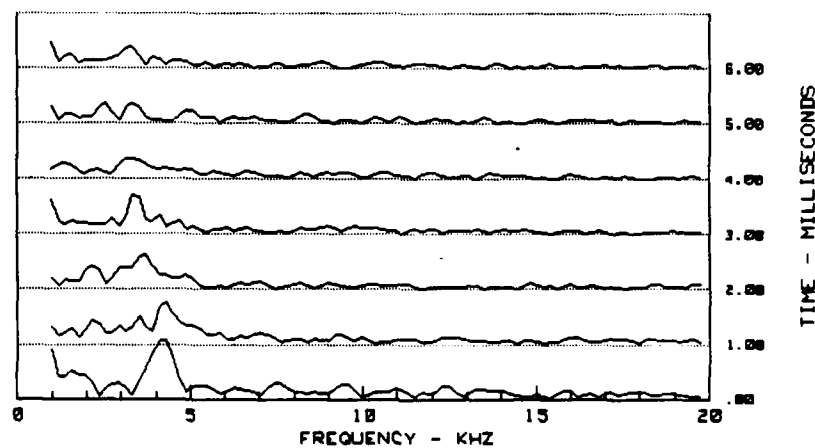
Figure A-10.   HV-VSA calibration (M = 1.67).

MAXIMUM FREQUENCY= 200 KHZ
FREQUENCY RESOLUTION= 195 HZ
TIME WINDOW= 2 millisec
NUMBER OF TIME POINTS= 2048
NUMBER OF DATA POINTS= 800
NUMBER OF ZERO FILLED POINTS= 1248
SAMPLE INTERVAL= 2.5 MICROSECONDS

Figure A-11.   HV-VSA calibration (u = 103.94 m/s).

56
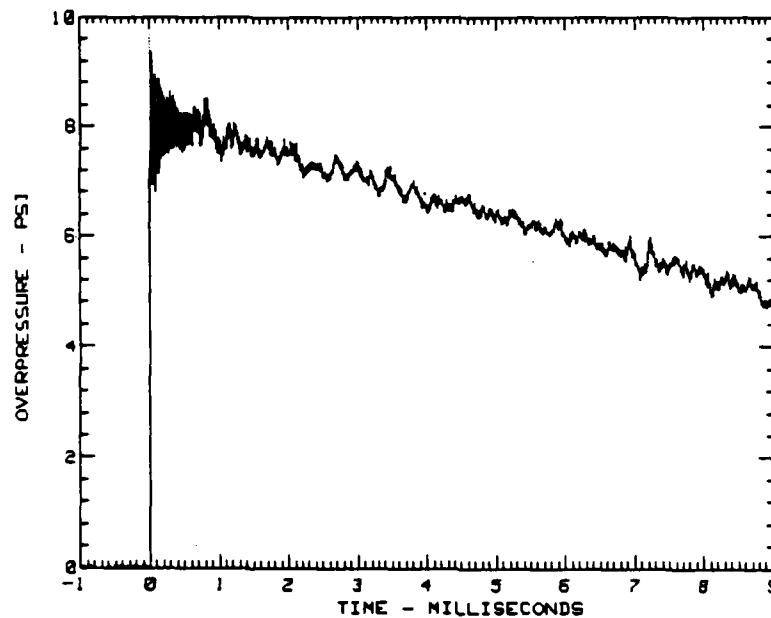
MAXIMUM FREQUENCY= 200 KHZ
FREQUENCY RESOLUTION= 195 HZ
TIME WINDOW= 2 millisec
NUMBER OF TIME POINTS= 2048
NUMBER OF DATA POINTS= 800
NUMBER OF ZERO FILLED POINTS= 1248
SAMPLE INTERVAL= 2.5 MICROSECONDS
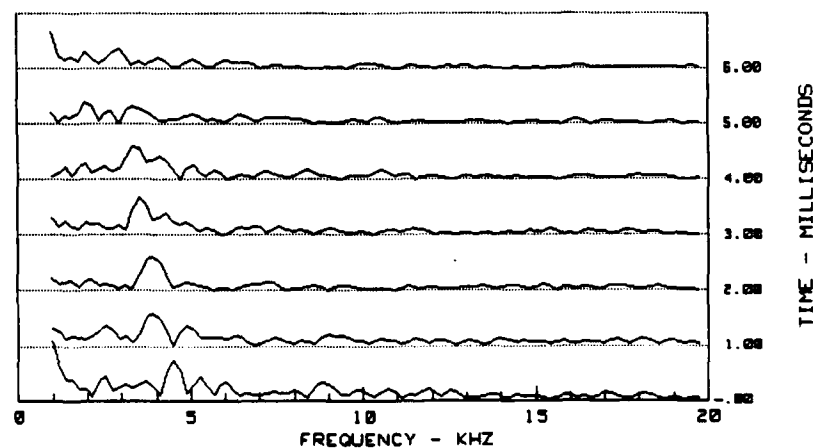
Figure A-12.   HV-VSA calibration (u = 112.47 m/s).

57

MAXIMUM FREQUENCY= 200 KHZ
FREQUENCY RESOLUTION= 195 HZ
TIME WINDOW= 2 millisec
NUMBER OF TIME POINTS= 2048
NUMBER OF DATA POINTS= 800
NUMBER OF ZERO FILLED POINTS= 1248
SAMPLE INTERVAL= 2.5 MICROSECONDS

Figure A-13.   HV-VSA calibration (u = 117.65 m/s).

58
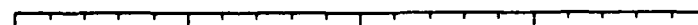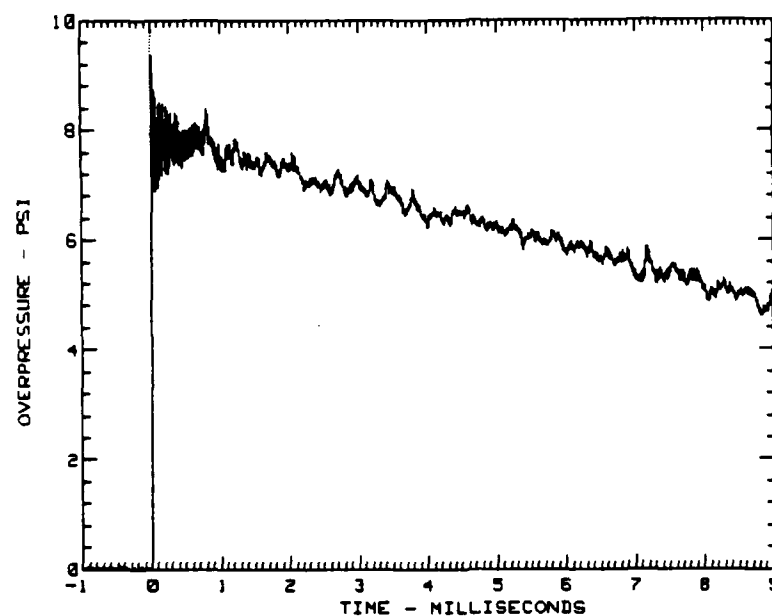
MAXIMUM FREQUENCY= 200 KHZ
FREQUENCY RESOLUTION= 195 HZ
TIME WINDOW= 2 millisec
NUMBER OF TIME POINTS= 2048
NUMBER OF DATA POINTS= 800
NUMBER OF ZERO FILLED POINTS= 1248
SAMPLE INTERVAL= 2.5 MICROSECONDS

Figure A-14.   HV-VSA calibration (u = 118.26 m/s).

MAXIMUM FREQUENCY= 200 KHZ
FREQUENCY RESOLUTION= 195 HZ
TIME WINDOW= 2 millisec
NUMBER OF TIME POINTS= 2048
NUMBER OF DATA POINTS= 800
NUMBER OF ZERO FILLED POINTS= 1248
SAMPLE INTERVAL= 2.5 MICROSECONDS

Figure A-15.   HV-VSA calibration (u = 230.73 m/s).

60
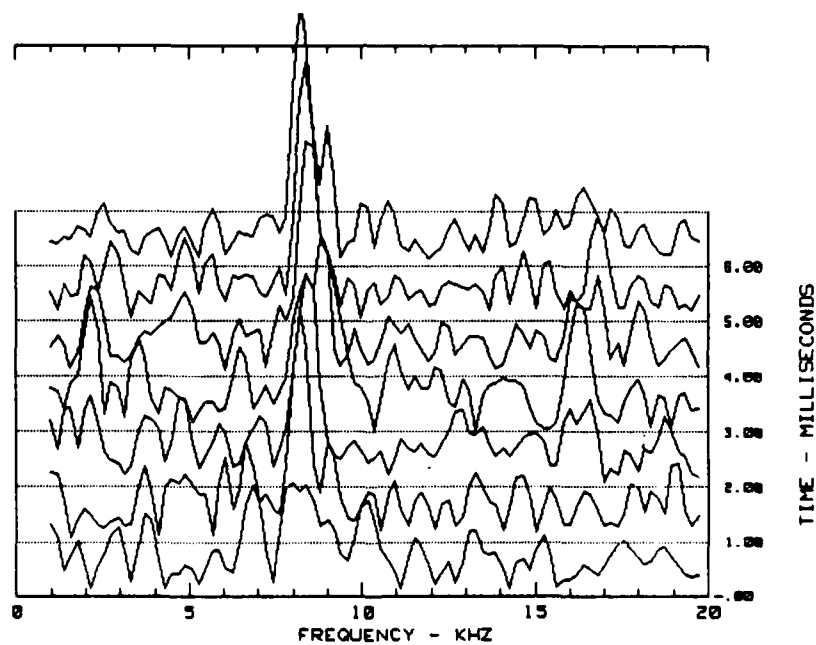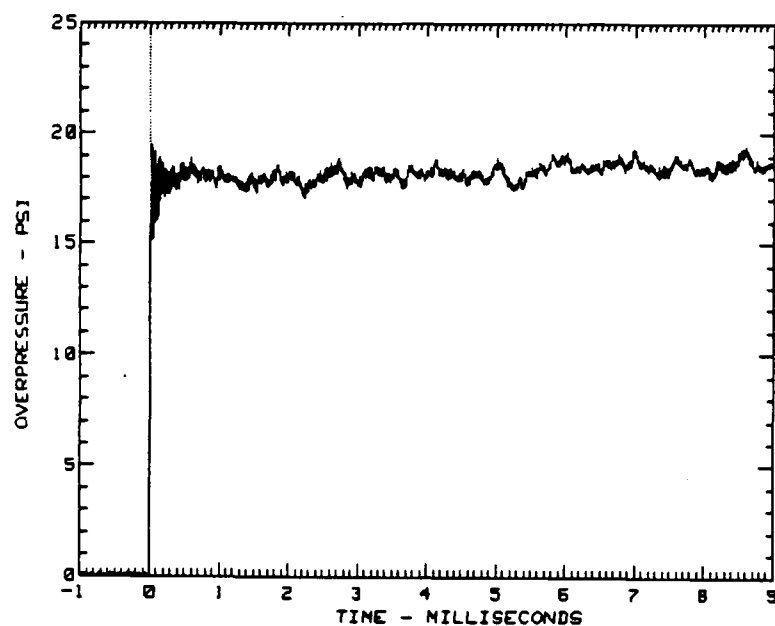
MAXIMUM FREQUENCY= 200 KHZ
FREQUENCY RESOLUTION= 195 HZ
TIME WINDOW= 2 millisec
NUMBER OF TIME POINTS= 2048
NUMBER OF DATA POINTS= 800
NUMBER OF ZERO FILLED POINTS= 1248
SAMPLE INTERVAL= 2.5 MICROSECONDS

Figure A-16.   HV-VSA calibration (u = 239.57 m/s).

61

MAXIMUM FREQUENCY= 80 KHZ
FREQUENCY RESOLUTION= 156 HZ
TIME WINDOW= 2 millisec
NUMBER OF TIME POINTS= 1024
NUMBER OF DATA POINTS= 320
NUMBER OF ZERO FILLED POINTS= 704
SAMPLE INTERVAL= 6.25 MICROSECONDS
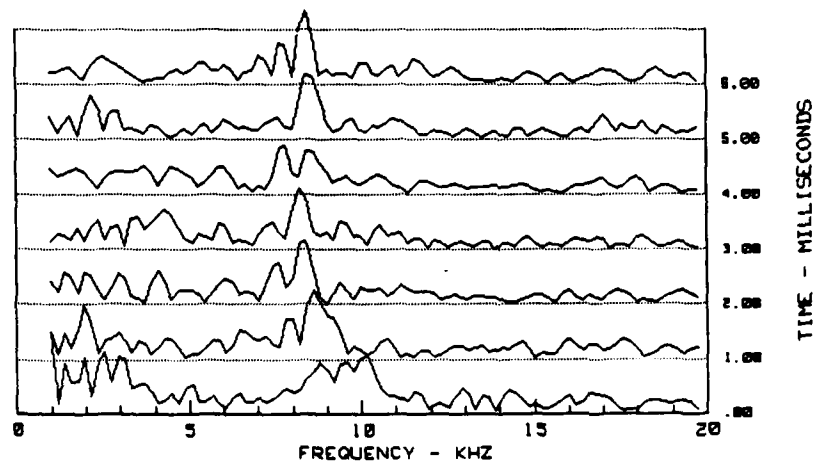
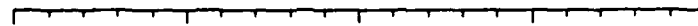Figure A-17.   HV-VSA calibration (u = 249.63 m/s).

MAXIMUM FREQUENCY= 200 KHZ
FREQUENCY RESOLUTION= 195 HZ
TIME WINDOW= 2 millisec
NUMBER OF TIME POINTS= 2048
NUMBER OF DATA POINTS= 800
NUMBER OF ZERO FILLED POINTS= 1248
SAMPLE INTERVAL= 2.5 MICROSECONDS
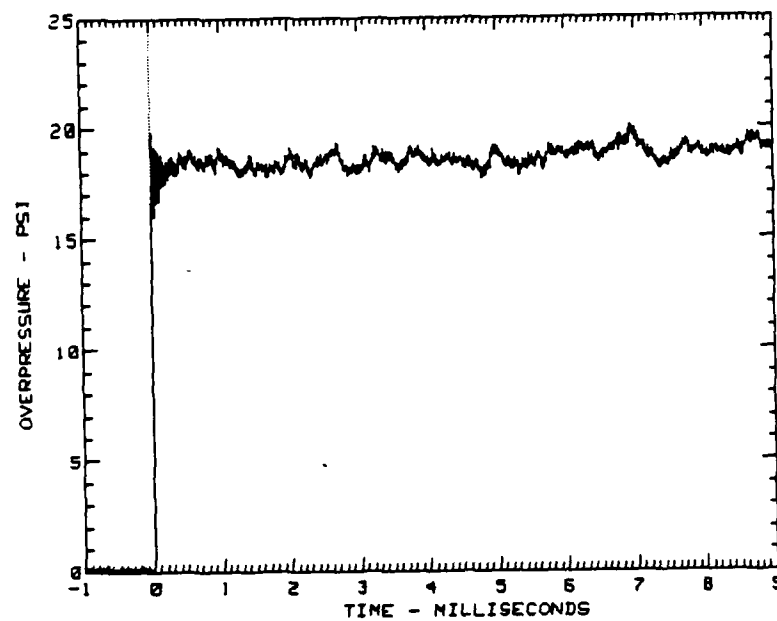
Figure A-18. HV-VSA calibration (u = 260.30 m/s).

63

MAXIMUM FREQUENCY= 200 KHZ
FREQUENCY RESOLUTION= 195 HZ
TIME WINDOW= 2 millisec
NUMBER OF TIME POINTS= 2048
NUMBER OF DATA POINTS= 800
NUMBER OF ZERO FILLED POINTS= 1248
SAMPLE INTERVAL= 2.5 MICROSECONDS
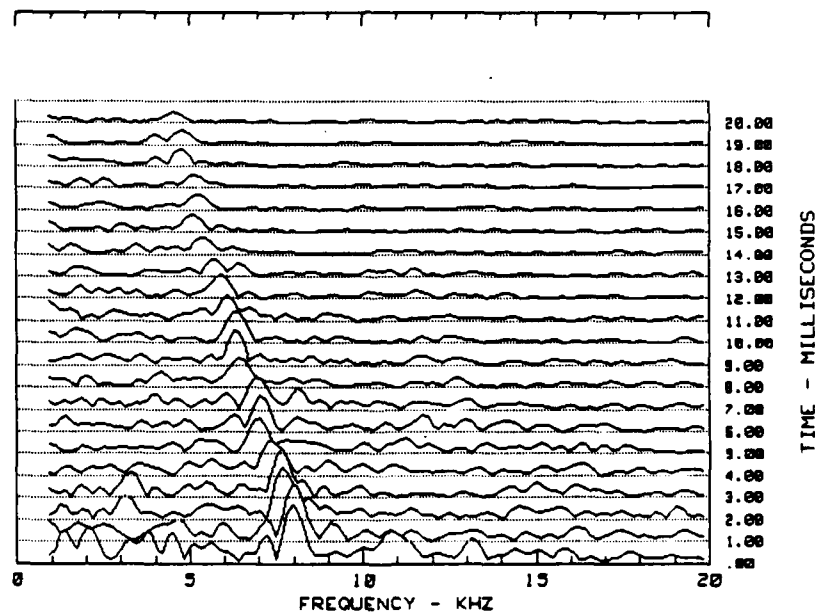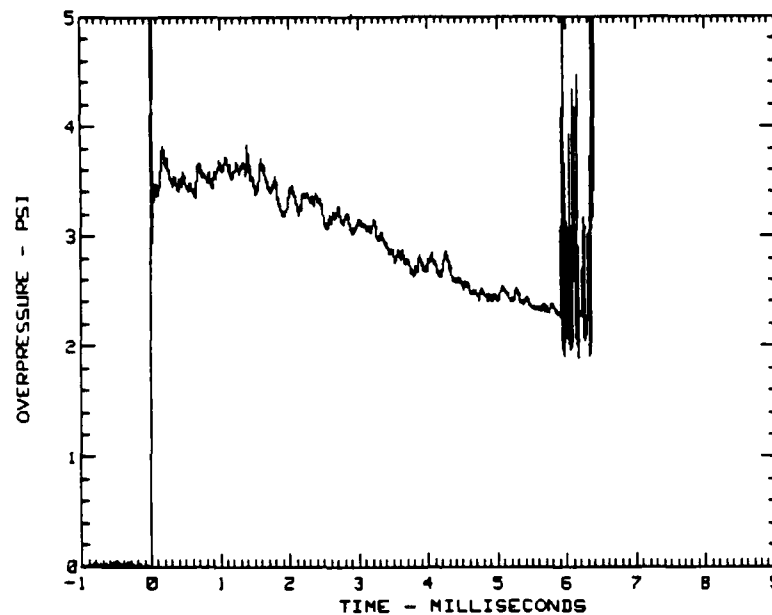
Figure A-19.   HV-VSA calibration (u = 383.13 m/s).

64
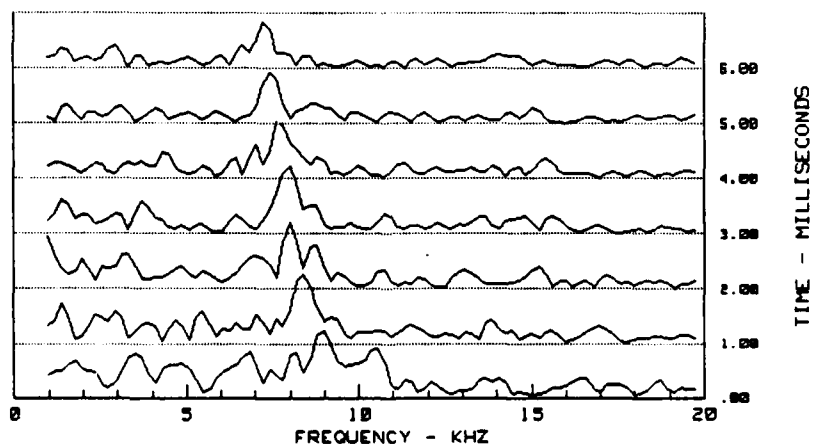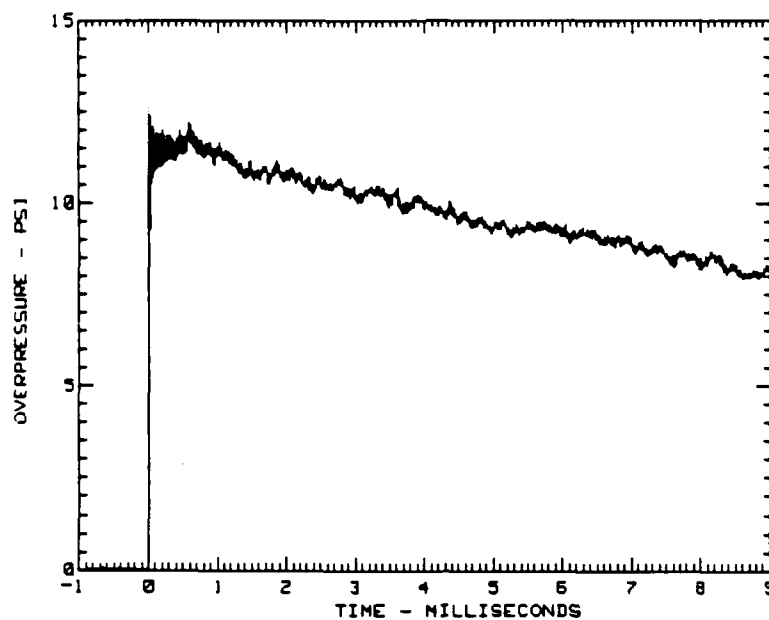
MAXIMUM FREQUENCY= 200 KHZ
FREQUENCY RESOLUTION= 195 HZ
TIME WINDOW= 2 millisec
NUMBER OF TIME POINTS= 2048
NUMBER OF DATA POINTS= 800
NUMBER OF ZERO FILLED POINTS= 1248
SAMPLE INTERVAL= 2.5 MICROSECONDS

Figure A-20.   HV-VSA calibration (u = 514.81 m/s).
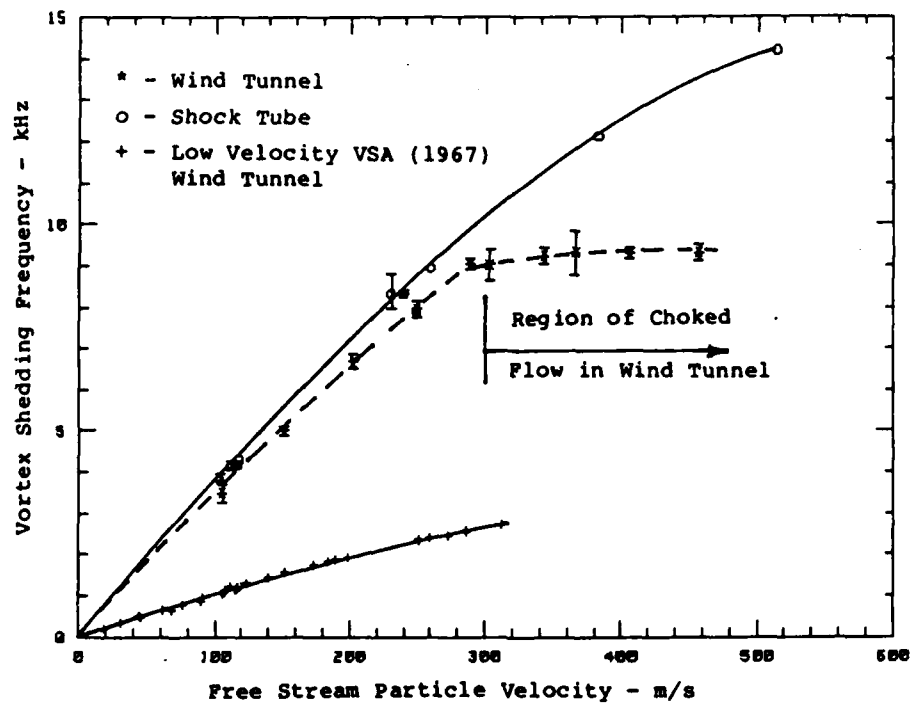
Figure A-21. Vortex shedding anemometer calibration.
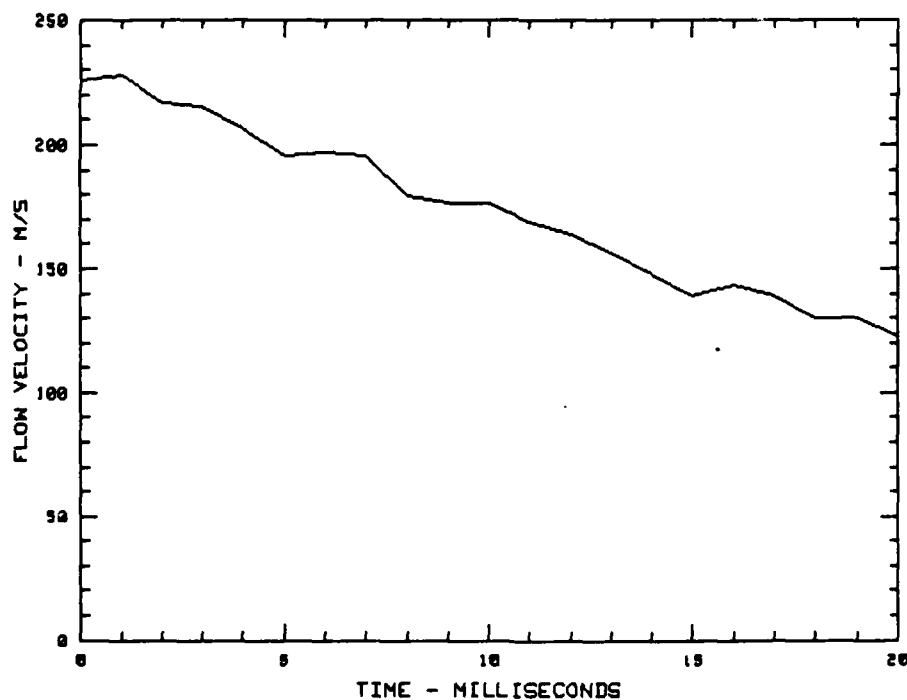
Figure A-22. Shock tube velocity profile for BRL, Shot 8.

66

APPENDIX B

FIELD TEST DATA

Four High Velocity Vortex Shedding Anemometers (HV-VSA) were fielded on event DIRECT COURSE at the 183 meter range. Three instruments in the dusty radial were installed at 5.1, 15.2 and 30.5 cm elevation respectively, while the clean radial measurement was 15.2 cm above the surface.

Each HV-VSA is equipped with two independent pressure transducers which can optionally be electrically connected in a differential sense, or they may be recorded separately. The latter option was selectd in view of the high probability of physical damage to the sensors.

One of the eight transducers was destroyed at shock arrival time. The other seven recorded channels are presented in this appendix along with spectral stack plots showing the frequency spectra of a two millisecond window tracking the data in one or two millisecond time steps.

As stated in the main text (Section 4), the data were contaminated with cross-talk effects by the multiplex system and no unambiguous signal can be identified in the data. Most of the peaks and trends in frequency seen can be attributed to contributions from the multiplex system as either FM sidebands or harmonic distortion caused by hetrodyning and/or interchannel modulation. Appendix C also is referenced for further discussion on the topic of multiplex noise.
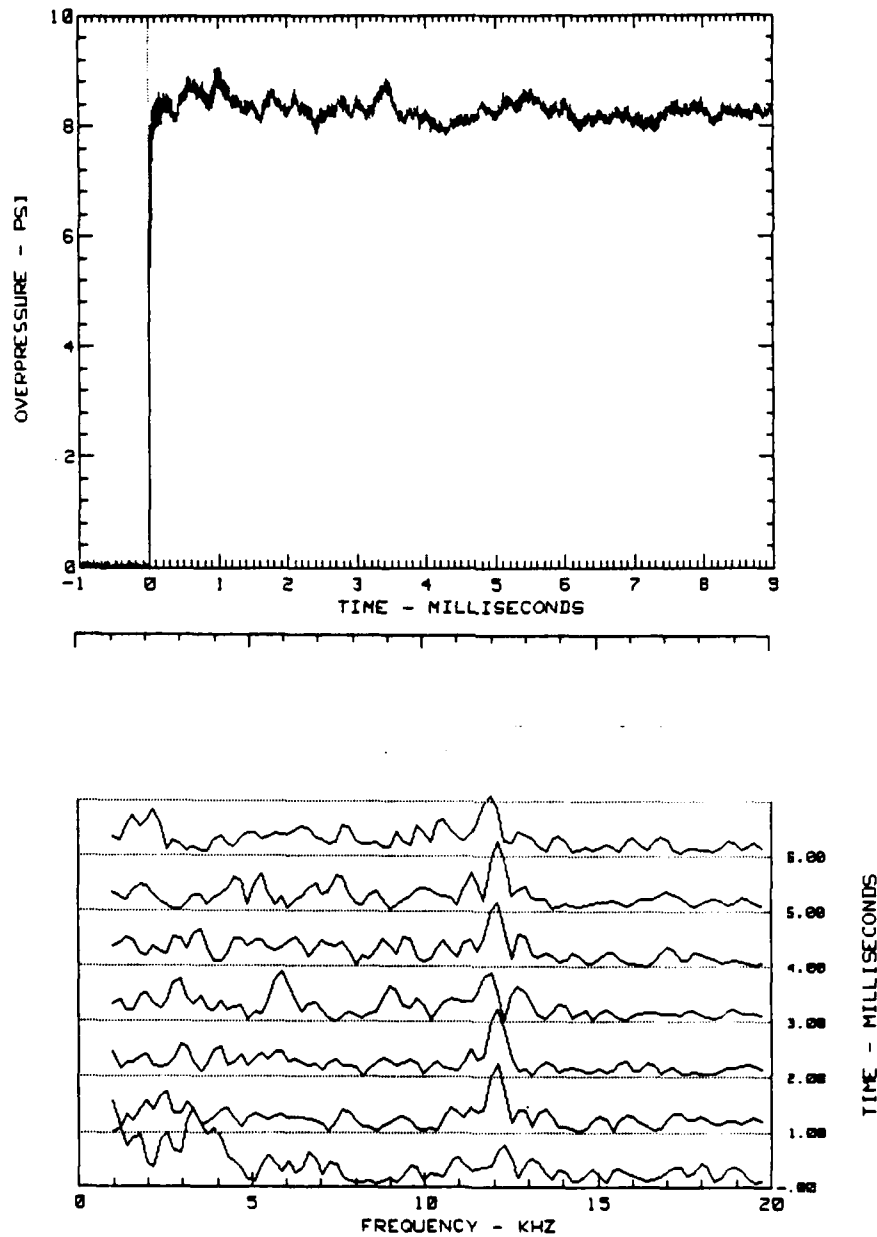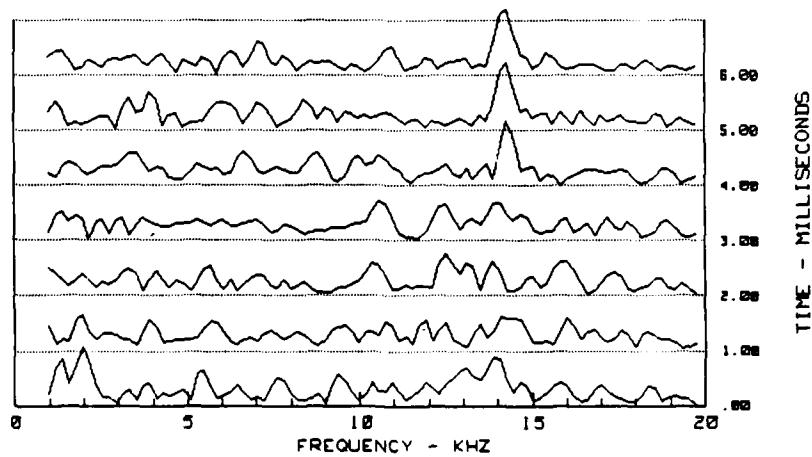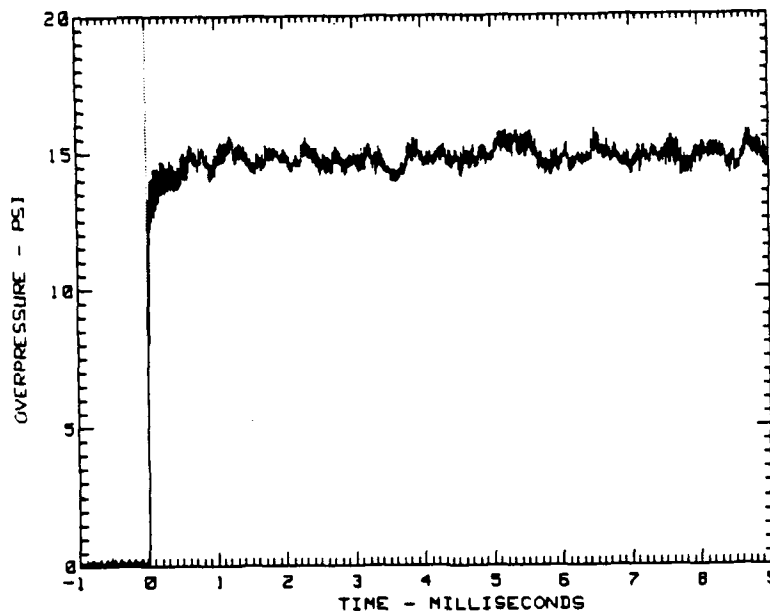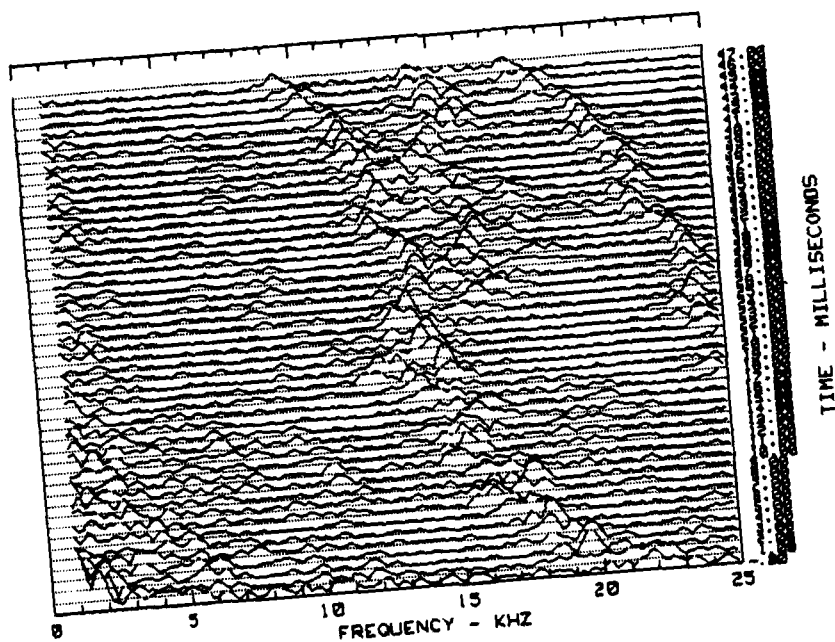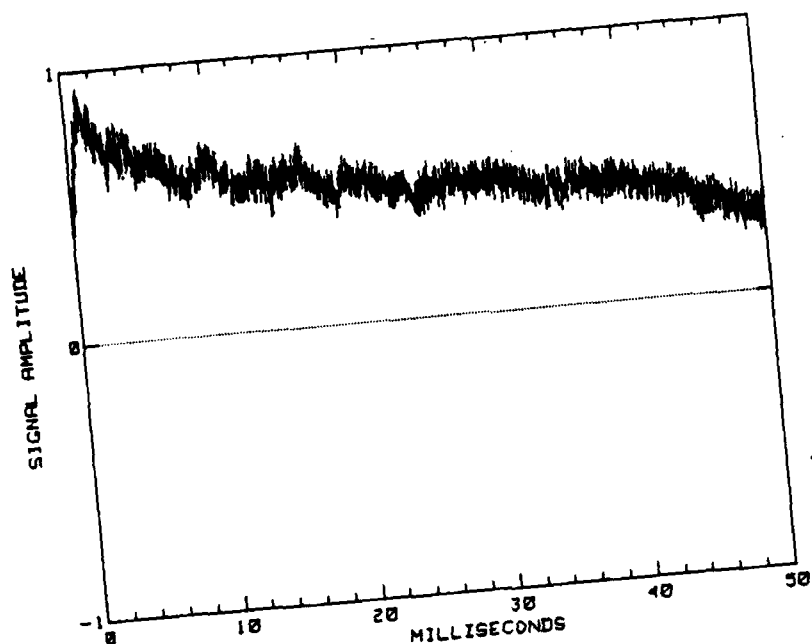
MAXIMUM FREQUENCY= 40 KHZ
FREQUENCY RESOLUTION= 156 HZ
TIME WINDOW= 2 MILLISEC
NUMBER OF TIME POINTS= 512
NUMBER OF DATA POINTS= 160
NUMBER OF ZERO FILLED POINTS= 352
SAMPLE INTERVAL= 12.5 MICROSECONDS

Figure B-1.   Channel 127-1-VL-L.
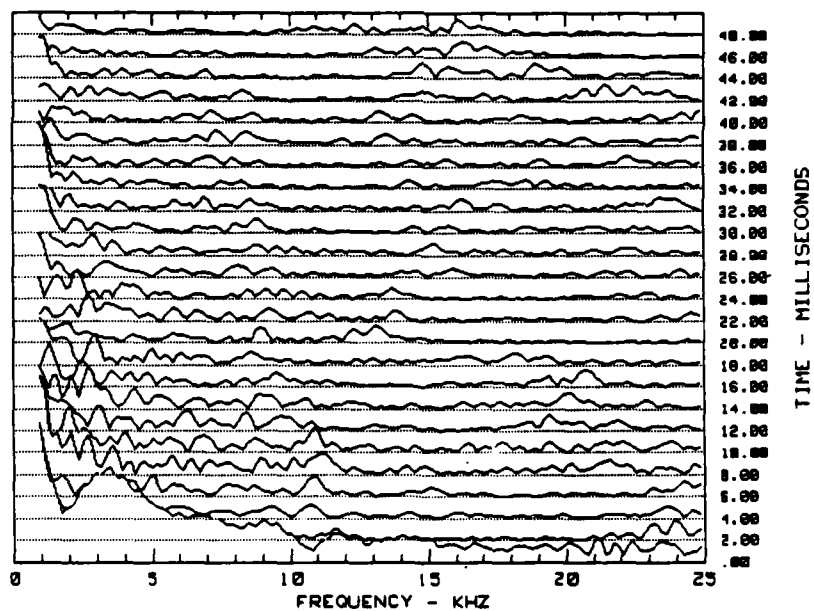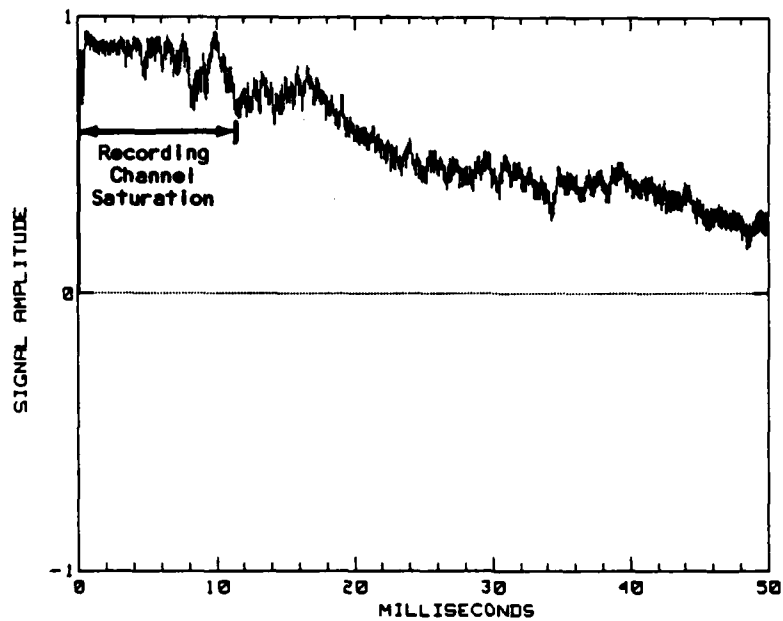
MAXIMUM FREQUENCY= 40 KHZ
FREQUENCY RESOLUTION= 156 HZ
TIME WINDOW= 2 MILLISEC
NUMBER OF TIME POINTS= 512
NUMBER OF DATA POINTS= 160
NUMBER OF ZERO FILLED POINTS= 352
SAMPLE INTERVAL= 12.5 MICROSECONDS

Figure B-2.   Channel 127-1-VL-R.
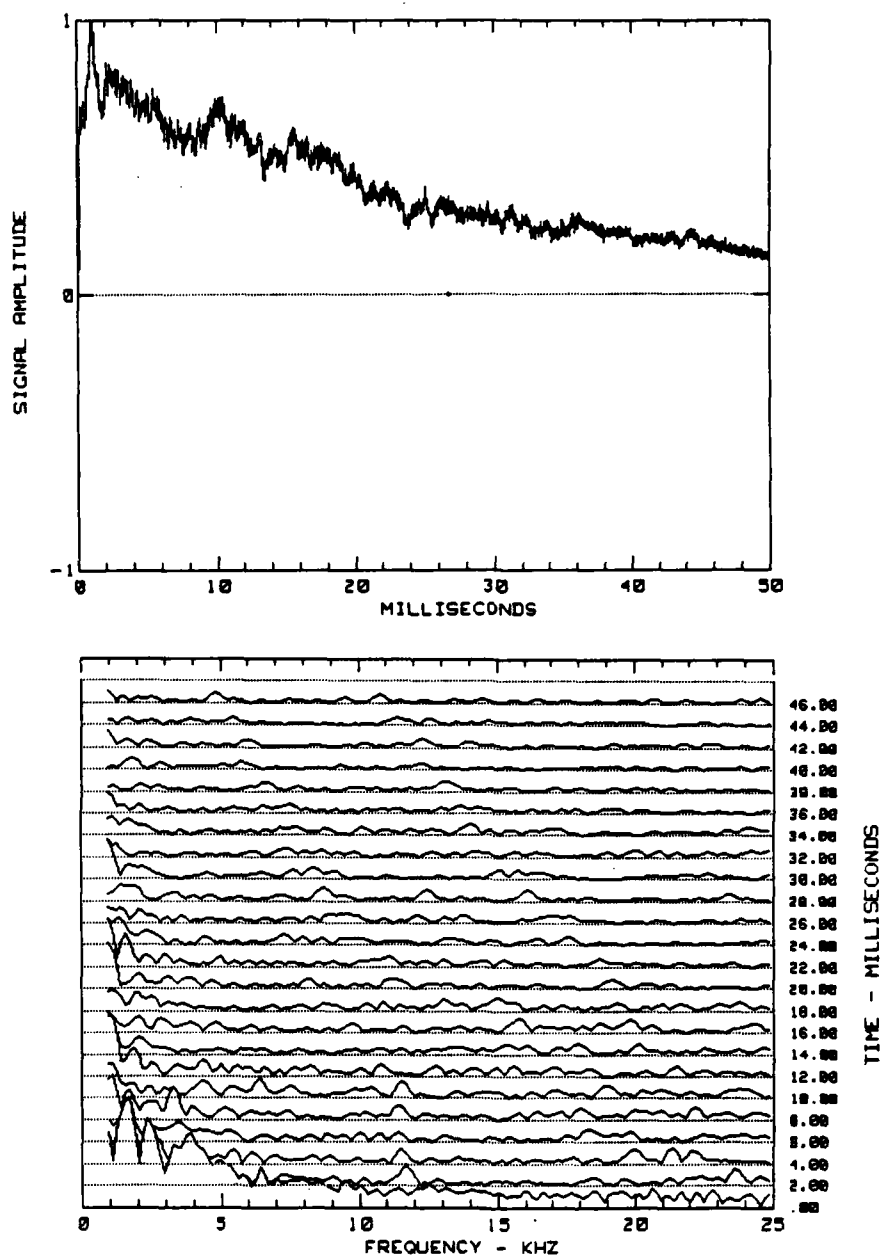
69

MAXIMUM FREQUENCY= 40 KHZ
FREQUENCY RESOLUTION= 156 HZ
TIME WINDOW= 2 MILLISEC
NUMBER OF TIME POINTS= 512
NUMBER OF DATA POINTS= 160
NUMBER OF ZERO FILLED POINTS= 352
SAMPLE INTERVAL= 12.5 MICROSECONDS

Figure B-3.   Channel 127-.5-VL-L.
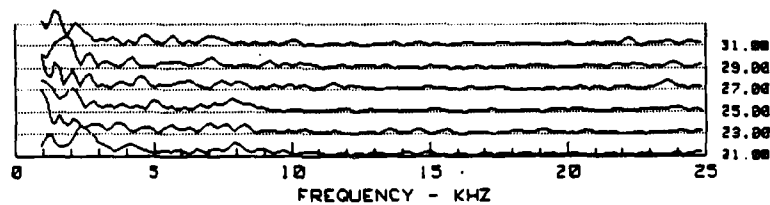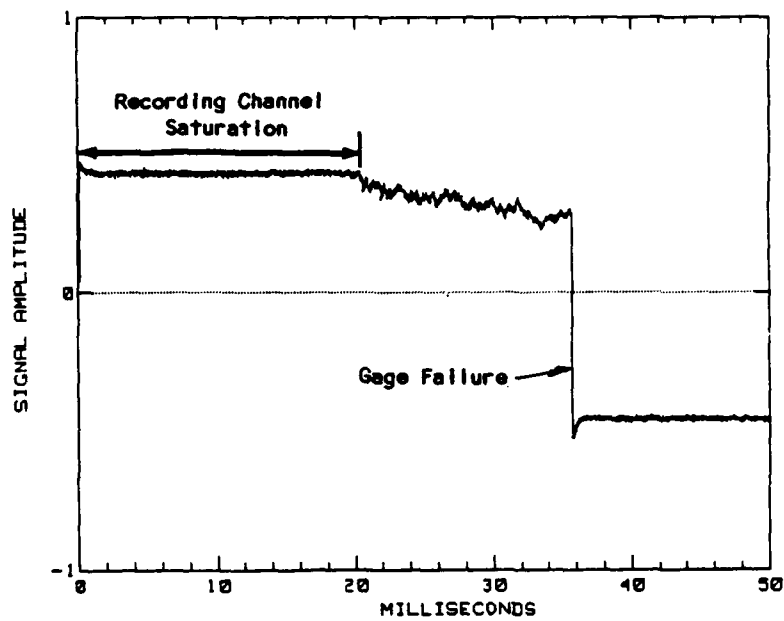
70

MAXIMUM FREQUENCY= 40 KHZ
FREQUENCY RESOLUTION= 156 HZ
TIME WINDOW= 2 MILLISEC
NUMBER OF TIME POINTS= 512
NUMBER OF DATA POINTS= 160
NUMBER OF ZERO FILLED POINTS= 352
SAMPLE INTERVAL= 12.5 MICROSECONDS

Figure B-4.   Channel 127-.5-VL-R.
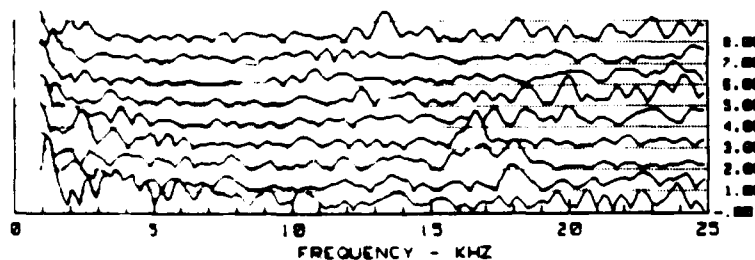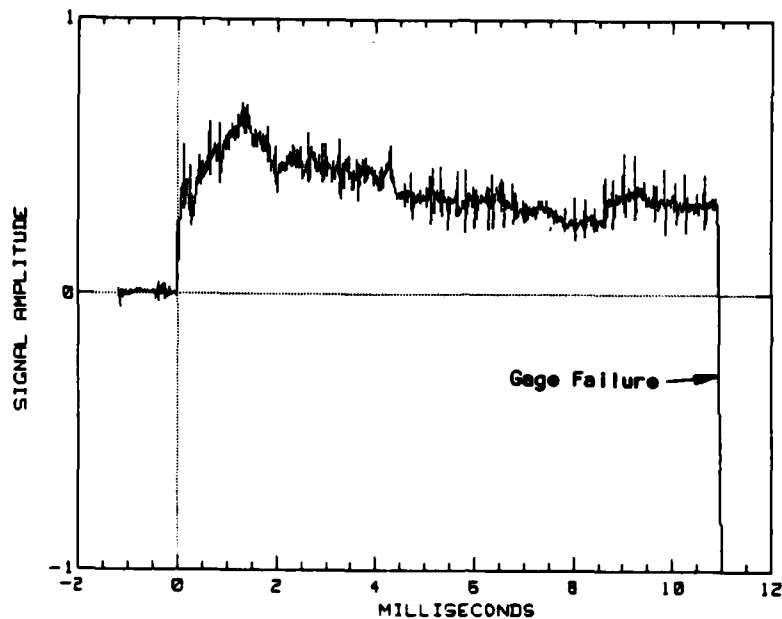
SIGNAL AMPLITUDE — MILLISECONDS

Gage Failure →

MAXIMUM FREQUENCY= 40 KHZ
FREQUENCY RESOLUTION= 196 HZ
TIME WINDOW= 2 MILLISEC
NUMBER OF TIME POINTS= 512
NUMBER OF DATA POINTS= 160
NUMBER OF ZERO FILLED POINTS= 352
SAMPLE INTERVAL= 12.5 MICROSECONDS

Figure B-5. Channel 127-.17-VL-L.
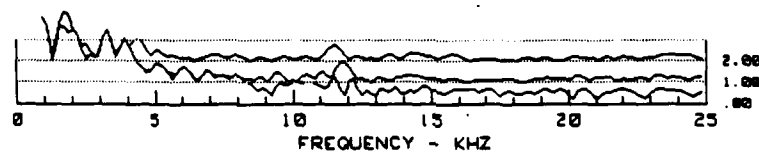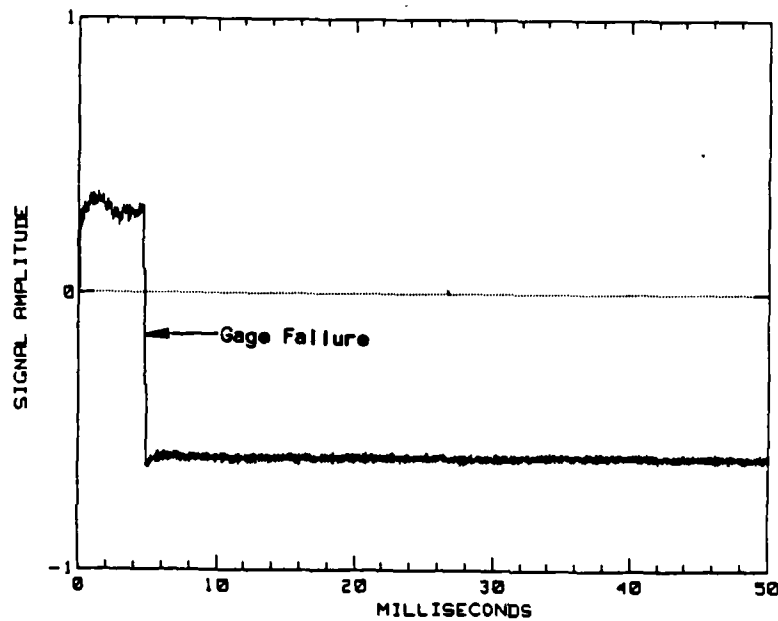
72

MAXIMUM FREQUENCY= 40 KHZ
FREQUENCY RESOLUTION= 156 HZ
TIME WINDOW= 2 MILLISEC
NUMBER OF TIME POINTS= 512
NUMBER OF DATA POINTS= 160
NUMBER OF ZERO FILLED POINTS= 352
SAMPLE INTERVAL= 12.5 MICROSECONDS

Figure B-6.   Channel 227-.5-VL-L.
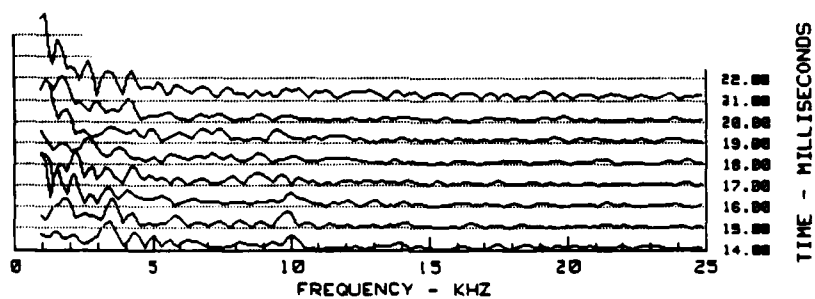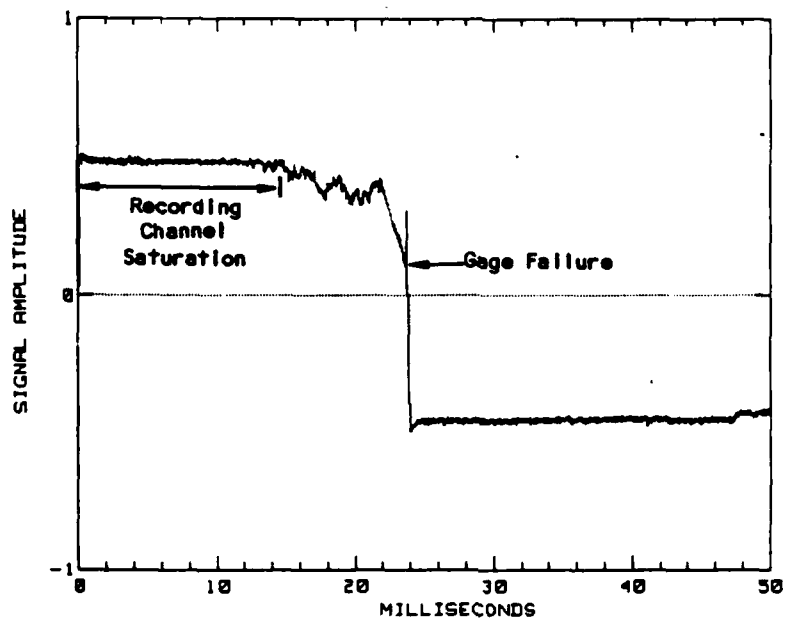
73

MAXIMUM FREQUENCY= 40 KHZ
FREQUENCY RESOLUTION= 156 HZ
TIME WINDOW= 2 MILLISEC
NUMBER OF TIME POINTS= 512
NUMBER OF DATA POINTS= 160
NUMBER OF ZERO FILLED POINTS= 352
SAMPLE INTERVAL= 12.5 MICROSECONDS

Figure B-7.   Channel 227-.5-VL-R.

APPENDIX C

FM MULTIPLEX RECORDING CONSIDERATIONS

This appendix addresses in detail the problem of interchannel modulation cross-talk that was encountered with the DIRECT COURSE VSA data.

A well known fact from fundamentals of frequency modulation (FM) theory is that the bandwidth required is approximately twice the maximum data frequency. The frequency sharing multiplex system used to record the DIRECT COURSE VSA data has 10 channels per multiplex group with center frequencies spaced 150 kHz apart starting at 250 kHz. The data bandwidth of 20 kHz is the same for all channels. Such a system is known as a constant bandwidth (CBW) multiplex (MUX) system. The FM signals from each channel are summed at the output of the MUX system to comprise a complex wideband signal that nominally ranges from 200 to 1750 kHz after the addition of an unmodulated reference frequency at 1750 kHz. Each MUX group consisting of 10 data channels requires one tape track of a wideband (2 mHz) analog instrumentation tape recorder.

As an example, consider the data channel with a center frequency of 250 kHz. Since the data bandwidth is given as 20 kHz, the channel carrier signal requires a bandwidth of 250 $\pm$ 40 kHz which places the upper limit at 290 kHz. Similarly, the adjacent channel has a lower frequency limit of 400 - 40 kHz or 360 kHz. Ideally, this leaves a 70 kHz guard band between each MUX channel and its adjacent neighbors. However, filters are not ideal and in fact the actual filters leak residual energy from one channel into the next.

The explanation presented is very simplistic in order to clearly portray the mechanism by which the VSA data were contaminated. Actually, the situation is much more complex with the FM carrier containing numerous side bands whose amplitude depends strongly on the modulation index. Other mechanisms also are present that allow generation of sum and difference frequencies between the various carriers. This topic is addressed in the paper on DINING CAR MUX problems. Excerpts from this paper follow in this appendix.

When data signal levels are adequate and the signal-to-noise ratio (SNR) is high, then the system performance, within design specifications, provides data of acceptable quality.

The information in the VSA signal is contained in the frequency of a signal that is superimposed on a signal that is proportional (approximately) to the overpressure. Thus, the recorder channel bandedge was determined by consideration of the static overpressure level rather than the amplitude of the vortex shedding signal fluctuations. This did not cause any problems during calibration of the VSA because the potential for cross-talk of the nature just described did not exist.

One final caveat in using MUX systems is that the other data channels in a MUX group are particularly vulnerable to interference caused by the nonlinear behavior of a VCO that is overdriven by large input signals that exceed the bandedge setting.

The remainder of Appendix C contains excerpts from a paper that was presented by KSC at the DNA Post-DINING CAR Instrumentation Results Meeting held at the DNA Test Directorate, Kirtland AFB, New Mexico on 29 and 30 July 1975. This paper entitled "A Critique on Noise Problems Associated with a Seven Channel FM Multiplex

Recording System" presents discussion and analysis of problems encountered by the KSC Field Sciences Laboratory during the course of fielding the same Vidar MUX system on an underground test event (UGT).

During the DINING CAR fielding period it was observed that in some cases, where noise was excessive on one or two channels within the MUX family of one track, the interference was traceable to a channel within an adjacent track MUX group.

An example of this was seen on tape 2-2 where the 1150 kHz, 1300 kHz and the 1450 kHz channels on track 12 exhibited interference modulation within the 20 kHz data band at the discriminator output. It should be noted that this unwanted signal was present and unaffected eventhough the VCO inputs for these channels were shorted and shunted to the ground. It was discovered that this signal could be eliminated by removing the corresponding (1150, 1300, or 1450 kHz) VCO from the track 14 MUX group.

The nature of this cross-talk was further investigated by connecting a spectrum analyzer to the recorder's direct reproduce output for track 12 with the discriminator input buss disconnected. Figure C-1 is an illustrated drawing that shows the test configuration and waveforms observed. A precision power supply was connected to the input of the VCO in question on track 14. As the voltage was varied from bandedge to bandedge, a shift of the parasitic frequency could be observed on the spectrum analyzer. Next, the single discriminator of the appropriate frequency was connected to the track 12 reproduce output. A frequency counter and an oscilloscope were patched into the discriminator output. At this point it could be observed that the discriminated output signal frequency was the difference frequency of the two corresponding carrier frequencies on different tracks. As the voltage

Figure C-1. Cross track heterodyning.

input to the VCO on track 14 was varied from zero to bandedge volts, the frequency output from the discriminator looking at the VCO of the same frequency channel on track 12 varied from 0 kHz to 40 kHz.

Deviation of the VCO carrier on either track caused the discriminated output to exhibit an approximate 20 dB signal at a frequency equal to the difference frequency between the two carriers on separate tracks.

The relative amplitude of this heterodyne signal could be reduced by lowering the amplitude of the carrier on the interfering channel (i.e. the amplitude of the heterodyne signal was proportional to the interfering carrier amplitude). The difficulty here lies in the fact that if the track 14 carrier amplitude is reduced sufficiently to lower the noise signal to an acceptable level on track 12 the SNR for the corresponding channel on track 14 is worsened since the pre-emphasis settings would be disturbed.

An effort to find and eliminate the point of heterodyning resulted in only minor improvement. The VCO rack mounts for tracks 12, 13, and 14 were Vidar type 9203-19, which requires an external MUX buss, while the other MUX track VCO mounts were type 9203-18. This was suspected as the possible problem source. Accordingly, these VCO mounts were replaced with the internal buss type mounts one at a time and checked.

While some improvement was observed, the difference frequency was reduced by 2 to 3 dB in each case, the basic problem was by no means eliminated.

Some notable observations can be made as associated with this problem.

1. This "cross-talk heterodyning" was the predominant noise source on one pair of tracks on each of the three recorders associated with multiplexing.

2. The tracks involved were, in all instances, even numbered tracks adjacent to each other on the head stack. They were not, however the same tracks in every case, e.g.

   tracks 2 and 4 on tape 1-1
   tracks 4 and 6 on tape 2-1
   tracks 12 and 14 on tape 2-2

3. The SNR produced on the higher frequency channels of these tracks was, in each instance, on the order of 20 dB.

   Note: At the expense of violating the pre-emphasis criterion the carrier levels on the interfering channels were reduced to attain a SNR of at least 26 dB on the corresponding channel of the adjacent track.

4. While this "cross-talk heterodyning" was detectable as noise on some other tracks the level was below that of other noise effects (i.e. 26 dB, SNR).

IMPROVEMENT OF SNR ON MULTIPLEX CHANNELS

Considerable expertise from several sources was brought to
bear upon the problem of cleaning up possible noise sources within
the MUX system. All possible noise sources, within reason, which
might be caused by faulty equipment or components, were diligently
rooted out, examined and corrected where necessary. All of the
MUX system components were meticulously set up as indicated by
the repair orders which were generated during that period. All of
this having been accomplished, test tapes were made on each system
which, when played back, seemed to indicate that the effort had
been successful.

Unfortunately, however, at the next use of each MUX system
on a dry run, the playback would show that many of the channels
still had SNRs on the order of 20 dB.

The obvious difference between the test tapes and the dry
run tapes was that instead of having the VCO inputs shorted they
were now connected to the incoming signal lines. However, the
signal lines had already been eliminated as the source of the
high noise levels. (The noise inherently found on the incoming
lines was measured as 0.05 mV peak-to-peak, high frequency "white
noise," all above the bandwidth capability of the recording system).
Even if this white noise had been recorded the SNR would have
been on the order of 32 to 36 dB. Note that throughout this
discussion SNR measurements refer to peak-to-peak noise relative
to bandedge-to-bandedge signal.

Two of the remaining differences between having the VCO inputs
shorted and having them connected to the signal lines is that
during the dry runs many of the gages give a sizable DC offset

82

and they receive calibration signals which are usually about 50% of bandedge, swinging positive for one step and negative for the other. It was observed that during the calibration steps several of the channels exhibited a dramatic increase in noise level. Further it was observed that if only one VCO was used in a system that it no longer exhibited the increase in noise during the cali- bration steps. Similarly it was demonstrated that if the system was held in a calibration step, while monitoring the discriminator output of a then-noisy channel, that the noise level diminished as the other VCOs within that MUX group were removed from the MUX buss. This confirms the earlier findings from MING BLADE postshot tests. (See DNA publication "Minutes of MING BLADE Instrumentation Results Meeting," page 36). The noise components in that text are termed "Intra-Carrier Modulation" and "Modulation Cross-Talk."

A further discussion of this phenomenon is found in Elliott L. Gruenberg's "Handbook of Telemetry and Remote Conrol," Chapter 6, page 10, under the heading Phase Modulation of One Carrier by Another, McGraw-Hill, 1967.

In brief: the superposition of two (or more) carrier fre- quencies when presented to the input of any nonlinear device will produce a modulation signal which will appear at the discriminator output as noise.

It follows that, since the tape recorder contains nonlinear functions which are influenced by the record level, the presence of modulation noise produced in this manner may be controlled to some degree by adjustment of the record level.

An oversight in the system setup procedure arises from the fact that all tracks were optimized for best SNR by adjusting the record level with all carriers set to their center frequency only. Obviously when any DC offset, calibration signal or data signal causes the VCOs to be deviated, all optimization is lost. Every new deviation point will produce a whole new family of superposition frequencies with a different set of modulation noise products.

Since the data on each channel are uniquely different in amplitude, frequency, phase, rate, etc., it would be ideal to optimize the record level for an infinite number of points. This being virtually impossible, a reasonable compromise may be had by adjusting to a point giving the minimum average noise between the plus calibration, negative calibration, and center band or offset deviation points.

Depending on the number of channels confronting the experimenter it may not be practical to establish such a "trade off" point while observing each channel of every track. Therefore some general "rule-of-thumb" procedures for this adjustment were established in actual practice.

In general:

1. For those tracks having all channels with no zero offset, observe the 550 kHz discriminator output with a scope and/or an rms reading AC voltmeter.

2. For those tracks having channels with large zero offsets, observe the 1300 kHz channel output.

3. Adjust the record level at each of the three deviation points to establish the minimum noise trade off point.

84

4. Each channel on the track may be observed briefly at this point while switching through the three deviation points to ensure that no channel has excessive noise at any given deviation level.

By using this method we were able to achieve a SNR of better than 26 dB on all channels of all tracks in the multiplex system.

MULTIPLEX SYSTEM CHANGES IMPLEMENTED ON DINING CAR

The following list of changes were implemented on DINING CAR as a consequence of poor quality multiplexed data recording on event MING BLADE. Items 1, 2 and 3 reduced crosstalk and inter-channel interference while items 4 and 5 influenced probability of success on any given measurement.

1. Reduced from ten to seven the number of channels in each MUX group. Eliminated troublesome carriers that
   a. interfere with other channels (400 kHz).
   b. are vulnerable to interference (1000 and 1600 kHz).

2. Confined the VCOs of each MUX group to a single rack mount.

3. Used pre-emphasis of carriers to distribute noise equally from upper to lower channels.

4. Assignment of carrier frequency according to gage type.
   a. Analog channels requiring best resolution assigned to the lower, least noise prone, carriers, e.g. strain gages on 250 kHz carriers.

   b. Digital data assigned to higher center frequency VCOs, e.g. velocity commutator on 1150 kHz.

5. Channel diversity arrangement improved.
   a. No single track carried all of the data from any gage type. A direct record board could malfunction resulting in the loss of data from all channels of one given type associated with one experiment.

b. No single track carried a majority of channels from any one experiment.

c. No single VCO rack mount carried a majority of the data from any one experiment or gage type. Failure of one rack mount power supply could result in the loss of seven channels.

OPERATION OF THE DINING CAR MULTIPLEX RECORDING SYSTEM

After the complete DINING CAR Multiplex System was set up and checked out, several test tapes were made. These test tapes were played back, discriminated and recorded on oscillographs both in the trailer and at the Bendix Playback Center. Once the two play-back systems were brought into reasonable agreement and the dif-ferences in operational compatibility were resolved, signal-to-noise measurements were made on each channel. These measurements indicated that, while some improvement in the system had been achieved over the system used on the previous UGT, it was also apparent that none of the innovations, not even the use of pre-emphasis, had proven to be a panacea for the multiplex noise problem.

It was not clear at this point which element of the MUX recording system was most likely to contain the noise source.

Although noise levels were generally lower at most tracks, the characteristic and type of noise was similar to that encountered on MING BLADE.

1. Lack of consistency from channel to channel and track to track.

2. Some channels exhibited a beat frequency running through the noise, while others have a fairly consistent amplitude at an apparent fixed frequency.

3. Some tracks exhibit random spiking.

4. Certain channels within a track appear to have frequency-modulated noise.

88

At this juncture (approximately two weeks prior to MFP), the Bendix Field Engineering tape maintenance crew put forth a major, concerted effort to find the source of noise in the MUX recording system and to assure that all associated equipment met or exceeded manufacturer's specifications.

The following is a compilation of relevant test procedures and setup operations performed by Bendix personnel:

1. Sangamo 4900 record boards setup for 1% 3rd harmonic at 10 kHz ref.

2. Set up 4900 record boards for 2 dB over bias.

3. Set up 4900 reproduce boards for $\pm$ 3 dB equalization.

4. Set pre-emphasis on each track. Using a spectrum analyzer, record and playback while adjusting each VCO for the same carrier amplitude relative to the noise floor.

5. Run complete systems and adjust record level on 4900 record boards for best signal to noise at highest MUX frequency.

6. Run complete system and take the following readings.
    a. Each MUX channel carrier level.
    b. Total MUX signal level per track.
    c. Level at record board, "record test jack."
    d. SNR at each MUX playback output.

7. Record a test tape with all MUX signals to be sent to playback center for check on SNR.

The conclusion reached by Bendix personnel was that there was no one thing that gave the bad signal-to-noise, it required that the complete system be setup in the right way.

89

DISTRIBUTION LIST

DEPARTMENT OF DEFENSE

Defense Intell Agcy
  ATTN: RTS-2A, Tech Lib
  ATTN: RTS-2B

Defense Nuclear Agency
  ATTN: SPAS, G. Ullrich
4 cys ATTN: STTI-CA

Defense Tech Info Ctr
12 cys ATTN: DD

Field Command, Defense Nuclear Agency
  ATTN: FCPR
  ATTN: FCTT
  ATTN: FCTT, W. Summa
  ATTN: FCTXE

Joint Strat Tgt Planning Staff
  ATTN: JLKS
  ATTN: JPTM

Under Secy of Def for Rsch & Engrg
  ATTN: Strat & Space Sys (OS)
  ATTN: Strat & Theater Nuc Forces, B. Stephan

DEPARTMENT OF THE ARMY

BMD Advanced Tech Ctr
  ATTN: ATC-T

BMD Systems Command
  ATTN: BMDSC-LEE, R. Webb

Harry Diamond Labs
  ATTN: DELHD-NW-P
  ATTN: DELHD-TA-L, Tech Lib

US Army Ballistic Rsch Lab
  ATTN: DRDAR-BLA-S, Tech Lib
  ATTN: DRDAR-BLT, J. Keefer

US Army Corps of Engineers
  ATTN: DAEN-ECE-T

US Army Engineer Ctr & Ft Belvoir
  ATTN: Tech Lib

US Army Engineer Div
  ATTN: HNDEN-FO

US Army Nuc & Chem Agcy
  ATTN: Library
  ATTN: MONA-WE, J. Uecke

DEPARTMENT OF THE NAVY

Naval Rsch Lab
  ATTN: Code 2627, Tech Lib
  ATTN: Code 4040, D. Book
  ATTN: Code 4040, J. Boris

Naval Surface Wpns Ctr
  ATTN: Code F31
  ATTN: Code R44, H. Glaz
  ATTN: Code X211, Tech Lib

DEPARTMENT OF THE NAVY (Continued)

Naval Surface Wpns Ctr
  ATTN: Tech Lib & Info Svcs Br

DEPARTMENT OF THE AIR FORCE

Air Force Institute of Technology
  ATTN: Library

Air Force Wpns Lab
  ATTN: NTED-A
  ATTN: SUL

Asst Ch of Staff, Studies & Analysis
  ATTN: AF/SAMI, Tech Info Div

Ballistic Missile Ofc/DAA
  ATTN: ENBF, D. Gage
  ATTN: ENSN
  ATTN: MGEN A. Schenker
  ATTN: PP

Strategic Air Command
  ATTN: NRI/STINFO

OTHER GOVERNMENT AGENCY

Central Intell Agcy
  ATTN: OSWR/NED

DEPARTMENT OF ENERGY CONTRACTORS

Los Alamos National Laboratory
  ATTN: C. Keller
  ATTN: M. Sandford
  ATTN: R. Whitaker

Sandia National Labs
  ATTN: Div 1111, J. Reed
  ATTN: J. Bannister
  ATTN: Org 7112, A. Chabai

DEPARTMENT OF DEFENSE CONTRACTORS

Acurex Corp
  ATTN: C. Wolf

Aerospace Corp
  ATTN: H. Mirels
  ATTN: Lib Acq MI/199

Applied Rsch Associates, Inc
  ATTN: J. Bratton
  ATTN: N. Higgins

Applied Rsch Associates, Inc
  ATTN: D. Piepenburg

Applied Theory, Inc
  ATTN: J. Trulio

Boeing Co
  ATTN: Aerospace Lib
  ATTN: S. Strack

California Rsch & Technology, Inc
    ATTN: K. Kreyenhagen
    ATTN: Library

California Rsch & Technology, Inc
    ATTN: F. Sauer

Carpenter Rsch Corp
    ATTN: H. Carpenter

University of Denver
    ATTN: Sec Ofcr for J. Wisotski

H&H Consultants, Inc
    ATTN: J. Haltiwanger
    ATTN: W. Hall

H-Tech Labs, Inc
    ATTN: B. Hartenbaum

Kaman Sciences Corp
    ATTN: R. Ruetenik

Kaman Sciences Corp
2 cys ATTN: E. Cole
2 cys ATTN: G. Roark

Kaman Tempo
    ATTN: DASIAC

Kaman Tempo
    ATTN: DASIAC

McDonnell Douglas Corp
    ATTN: D. Dean
    ATTN: H. Herdman
    ATTN: R. Halprin

Mission Rsch Corp
    ATTN: C. Longmire

University of New Mexico
    ATTN: G. Leigh
2 cys ATTN: D. Calhoun

University of New Mexico
    ATTN: J. Kovarna

Nichols Rsch Corp, Inc
    ATTN: N. Byrn

Pacific-Sierra Rsch Corp
    ATTN: H. Brode, Chairman SAGE

Pacific-Sierra Rsch Corp
    ATTN: D. Gormley

Pacifica Technology
    ATTN: R. Allen
    ATTN: Tech Library

Patel Enterprises, Inc
    ATTN: M. Patel

Physical Rsch, Inc
    ATTN: R. Deliberis
    ATTN: W. Mendes

Physics International Co
    ATTN: H. Wampler

R&D Associates
    ATTN: A. Kuhl
    ATTN: P. Haas
    ATTN: Tech Info Ctr

Rand Corp
    ATTN: B. Bennett

S-CUBED
    ATTN: C. Dismukes
    ATTN: J. Barthel
    ATTN: K. Pyatt
    ATTN: Library

S-CUBED
    ATTN: C. Needham

Science & Engrg Associates, Inc
    ATTN: B. Chambers, III

Science Applications International Corp
    ATTN: G. Binninger

Science Applications Intl Corp
    ATTN: H. Wilson
    ATTN: R. Schlaug
    ATTN: Tech Lib

Science Applications Intl Corp
    ATTN: J. Cockayne
    ATTN: W. Layson

SRI International
    ATTN: G. Abrahamson
    ATTN: J. Colton
    ATTN: Library

Teledyne Brown Engineering
    ATTN: B. Hartway
    ATTN: D. Ormond
    ATTN: F. Leopard

TRW Electronics & Defense Sector
    ATTN: N. Lipner
    ATTN: Tech Info Ctr

TRW Electronics & Defense Sector
    ATTN: E. Wong
    ATTN: G. Hulcher
    ATTN: P. Dai

Weidlinger Assoc, Consulting Engrg
    ATTN: I. Sandler

END

FILMED

1-86

DTIC